Mon. Not. R. Astron. Soc. **394,** 2001–2021 (2009) doi:10.1111/j.1365-2966.2009.14441.x

Modelling the effects of dust evolution on the SEDs of galaxies of different morphological type

A. Schurer,[1,2]★ F. Calura,[3] L. Silva,[3] A. Pipino,[4] G. L. Granato,[3] F. Matteucci[3,5] and R. Maiolino[6]

[1]*Astrophysics Sector, SISSA/ISAS, Via Beirut 2-4, I-34014 Trieste, Italy*
[2]*INAF, Osservatorio Astronomico di Padova, Vicolo dell'Osservatorio 5, I-35122 Padova, Italy*
[3]*INAF, Osservatorio Astronomico di Trieste, Via G. B. Tiepolo 11, I-34131 Trieste, Italy*
[4]*Astrophysics, University of Oxford, Denys Wilkinson Building, Keble Road, Oxford OX1 3RH*
[5]*INAF, Dipartimento Astronomico-Universita di Trieste, Via G. B. Tiepolo 11, I-34131 Trieste, Italy*
[6]*INAF – Osservatorio Astronomico di Roma, Via di Frascati 33, Monte Porzio Catone, Italy*

Accepted 2008 December 23. Received 2008 November 26; in original form 2008 July 10

ABSTRACT

We present photometric evolution models of galaxies, in which, in addition to the stellar component, the effects of an evolving dusty interstellar medium have been included with particular care. Starting from the work of Calura et al., in which chemical evolution models have been used to study the evolution of both the gas and dust components of the interstellar medium in the solar neighbourhood, elliptical and irregular galaxies, it has been possible to combine these models with a spectrophotometric stellar code that includes dust reprocessing (GRASIL) to analyse the evolution of the spectral energy distributions (SEDs) of these galaxies. We test our models against observed SEDs both in the local universe and at high redshift, and use them to predict how the percentage of reprocessed starlight evolves for each type of galaxy. The importance of following the dust evolution is investigated by comparing our results with those obtained by adopting simple assumptions to treat this component.

Key words: ISM: abundances – dust, extinction – galaxies: evolution – galaxies: ISM.

1 INTRODUCTION

Small solid grains of material present within the interstellar medium (ISM) of galaxies, often referred to as dust, absorb and scatter stellar radiation mainly in the ultraviolet (UV) and optical, re-emitting it in the infrared (IR). This process has been receiving increasing interest due to the development of sophisticated satellites operating in the IR [initially *IRAS*, *Infrared Space Observatory (ISO)* and more recently *Spitzer*] and large Earth-bound telescopes [e.g. Submillimetre Common-User Bolometer Array (SCUBA), a detector on the James Clerk Maxwell Telescope operating in the submillimetre] which have indisputably demonstrated the importance of these particles. Indeed, it has been found that approximately 30 per cent of all light radiated by stars in the local universe has been dust reprocessed (Soifer & Neugebauer 1991), and measurements of the far-infrared (FIR)/submillimetre background estimate a potentially larger percentage ∼50 per cent reprocessed over the entire history of the universe (see e.g. Hauser & Dwek 2001 for a review).

Hence, a proper treatment of the dust reprocessing in galaxies is essential, both to derive physical quantities, such as star formation rates (SFRs) and star formation histories from observations, and also when testing theoretical galaxy formation models against observations. To do this, it is necessary to model the effect that the ISM has on the propagation of photons from the stellar sources to the edge of the galaxy. As a result, a good knowledge of the properties of the dust component and its distribution within a galaxy is required.

Observations from our own galaxy have provided insights into the composition of interstellar dust, its morphology, size distribution and relative abundance of its various elemental constituents, and many viable models have been proposed to explain them. The most commonly used dust compositions include those of Mathis, Rumple & Nordsieck (1977), Draine & Lee (1984), Draine & Li (2001, 2007), Weingartner & Draine (2001), Desert, Boulanger & Puget (1990) and Zubko, Dwek & Arendt (2004). Such compositions try to recreate the amount of extinction observed to local stars, the emission from local dust clouds and the depletion of elements.

Several galactic dust models have been proposed to follow the propagation of photons through the ISM (see reviews by Dopita 2005 for starbursts, Popescu & Tuffs 2005 for normal galaxies and Madden 2005 for irregular galaxies). Such galactic dust models treat this component with differing geometries and with varying degrees of sophistication. Some, which solely involve radiative transfer calculations, have been used to account for the optical appearance of galaxies (Xilouris et al. 1997, 1998, 1999; Bianchi

★E-mail: schurer@sissa.it

© 2009 The Authors. Journal compilation © 2009 RAS

Downloaded from https://academic.oup.com/mnras/article/394/4/2001/1203297 by guest on 20 August 2022

2007), some have only used dust emission models to account for the FIR/submillimetre SEDs (Dale et al. 2001; Draine & Li 2007) and some which combine radiative transfer with a dust model in order to self-consistently model SEDs from the UV to the submillimetre and radio (Silva et al. 1998, hereafter S98; Bianchi, Davies & Alton 2000; Efstathiou, Rowan-Robinson & Siebenmorgan 2000; Efstathiou & Rowan-Robinson 2003; Tuffs et al. 2004; Piovan, Tantalo & Chiosi 2006).

Many of the proposed models are based on the dust composition models calculated for the Milky Way, and for simplicity use this same dust composition for all morphological types of galaxies and for every stage of their evolution. However, unsurprisingly, observations indicate that dust properties are likely to vary with age and morphological type. For example, observations of very high redshift and hence young galaxies (Maiolino et al. 2004) and dwarf irregular galaxies (e.g. Galliano et al. 2005) have been used to infer very different sizes and compositions of dust grains in these galaxies than those observed in the Milky Way. So it is unlikely to be sufficient to model the effects of dust at all redshifts and in galaxies with very different properties, and star formation histories using only one-grain distribution model. It is also common to calculate the total mass of dust by assuming a dust-to-gas mass ratio proportional to the metallicity of the galaxy, with the same constant of proportionality in all environments (e.g. Granato et al. 2000; Baugh et al. 2005). An assumption which is far from certain, for example much lower than expected dust-to-gas ratios have been found in several dwarf irregular galaxies (Galliano et al. 2003, 2005; Hunt, Bianchi & Maiolino 2005). Hence, it would be beneficial when modelling the effects of dust reprocessing in a range of different environments to be able to relax these assumptions and select appropriate dust properties for each galaxy individually. Unfortunately, observational evidence regarding the exact dust composition outside our own galaxy is very limited. It is therefore necessary at the present time in order to model SEDs of galaxies of different type and at different stages in their evolution to rely on theoretical models which follow the evolution of dust.

The dust grains are believed to be formed in a wide range of astrophysical processes, particularly in the stellar outflow of giant and Wolf–Rayet stars. Recent FIR to submillimetre observations of quasars have revealed large masses of dust at high redshift (Bertoldi et al. 2003; Robson et al. 2004; Beelen et al. 2006). The presence of such quantities of dust when the universe was $\leq$1-Gyr-old before significant dust production from giant stars was possible suggests that an important role should be played by the enrichment due to supernovae (SNe) (Morgan & Edmunds 2003; Maiolino et al. 2004; Dwek, Galliano & Jones 2007), and the observation of dust in the remnants of SNe (Dunne et al. 2003, 2008; Morgan et al. 2003 but see also Krause et al. 2004; Wilson & Batrla 2005; Sugerman et al. 2006) have provided further evidence for the formation of dust in these objects. However, this process is complicated by the destruction of SNe dust grains by the reverse shock propagating through the SNe ejecta. Once injected into the ISM, the grains are subjected to a variety of interstellar processes including thermal sputtering in high-velocity shocks, evaporation and shattering by grain–grain collisions and accretion in dense molecular clouds (MCs).

The challenge facing a dust evolution model is therefore to combine all of these processes in one model and use it to recreate several observation particularly the dust depletion levels observed in the local universe, examples include Dwek (1998), Calura, Pipino & Matteucci (2008, hereafter CPM08), Zhukovska, Gail & Trieloff (2008).

This work aims to combine the two different areas by using two well-tested models, the chemical and dust evolution model of CPM08 to follow the chemical and dust grain evolution of galaxies of different morphology and then use the GRASIL code (S98) to use the calculated stellar and dust evolution in order to calculate the SED expected for the galaxy. The importance of following the dust evolution is tested by comparing these fiducial SEDs with SEDs generated by adopting two common simplifications: that the dust-to-gas mass ratio is proportional to the metallicity, and that the dust composition in all galaxies is equal to that derived for the Milky Way. The main goal of this paper will be a quantitative comparison between the SEDs generated using the fiducial model and that by adopting the simplifications. In such a way, it is possible to estimate what errors could theoretically be expected from adopting such assumptions.

We test our models of the three morphologies (spirals, irregulars and ellipticals) against observed SEDs in the local universe (Dale et al. 2007) and the model elliptical galaxies at early times against observations of their expected high-redshift counterparts, SCUBA galaxies (Clements et al. 2008) and massive post-starburst galaxies at high redshift (Wiklind et al. 2008). We also use the models to predict how the percentage of reprocessed starlight evolves for each type of galaxy.

In this work, it was only possible to follow in detail the evolution of the chemical composition of the dust and not how the size distribution and chemical makeup of the individual grains evolve, a potentially large but for now unavoidable limitation. To test this, alternative size distributions for the irregular galaxy and for the young starbursting elliptical galaxy were proposed based on observed extinction curves, and the resultant SEDs are presented.

The plan of our paper is as follows. In Section 2, the chemical and dust evolution model is explained; in Section 3, the spectrophotometric dust model is introduced and the choices of parameters are discussed; in Section 4, the integration of the two models is briefly described; in Section 5, the calculated SEDs are presented and are compared to observations, in addition a quantitative comparison is made between them and the SEDs generated using the simple dust assumptions; in Section 6, the implications of our work are discussed. Some concluding remarks are given in Section 7.

2 CHEMICAL EVOLUTION MODELS

The chemical evolution models that this paper is based upon are presented in the CPM08 paper. These models follow the chemical evolution of several different elements in both the gas and the dust components of the ISM, of spiral, elliptical and irregular galaxies. More detailed descriptions of these models can be found in Matteucci & Tornambè (1987), Matteucci (1994) and Pipino et al. (2002, 2005) for the elliptical galaxies, Chiappini, Matteucci & Gratton (1997) and Chiappini, Matteucci & Romano (2001) for the spirals and Bradamante, Matteucci & D'Ercole (1998) for irregular galaxies. For convenience, the main details will be summarized here.

2.1 Gas evolution

All the models consider only one gas phase. In all models, the instantaneous recycling approximation is relaxed and the stellar lifetimes are taken into account. The abundance of several of the elements in the gaseous phase of the ISM (H, He, Li, C, N, O, α-elements, Fe, Fe peak elements and S-process elements) is

Downloaded from https://academic.oup.com/mnras/article/394/4/2001/1203297 by guest on 20 August 2022

followed from the birth of the galaxy. The following processes are considered.

(i) The subtraction of elements from the gaseous phase of the ISM due to star formation.

(ii) The production in stellar winds in low- and intermediate-mass non-binary stars with masses 0.8–8 $M_\odot$.

(iii) The production in Type Ia SNe by binary stars in systems with combined masses 3–16 $M_\odot$.

(iv) The production in Type II SNe of massive stars of masses 8–100 $M_\odot$.

(v) The increase in primordial elements due to infalling gas.

(vi) The loss of elements from gas outflows due to galactic wind as the thermal energy of the gas exceeds its binding energy (only present in the irregular and elliptical models).

Low- and intermediate-mass stars contribute to the ISM metal enrichment through quiescent mass loss and a planetary nebula phase by adopting prescriptions by van den Hoek & Groenwegen (1997). For massive stars and Type Ia SNe, the empirical yields suggested by François et al. (2004) are adopted.

The star formation efficiencies and the rate of infall in addition to the initial mass function (IMF) are selected for each of the galaxy morphologies in order to reproduce observed chemical abundances.

2.1.1 Spirals

The galactic disc is approximated by several independent rings, 2 Kpc wide, without interchange of matter between them. In this picture, spiral galaxies are assumed to form as a result of two main infall episodes. During the first episode, the halo and the thick disc are formed. During the second episode, a slower infall of external gas forms the thin disc with the gas accumulating faster in the inner than in the outer region, with time-scales equal to about 1 and 8 Gyr, respectively (the inside-out scenario). The SFR is given by the expression

$$\psi(r,t) = \nu \left[\frac{\sigma(r,t)}{\sigma(\mathrm{r}_\odot,t)}\right]^{2(k-1)} \left[\frac{\sigma(r,t_{\mathrm{Gal}})}{\sigma(r,t)}\right]^{k-1} \sigma^k_{\mathrm{ISM}}(r,t), \quad (1)$$

where $\sigma(r,t)$ is the total mass (gas + stars) surface density at a radius r and time t, $\sigma(\mathrm{r}_\odot, t)$ is the total mass surface density in the solar region. The star formation efficiency, ν, is set to $\nu = 1\,\mathrm{Gyr}^{-1}$ and becomes zero when the surface density drops below $\sigma_{\mathrm{th}} = 7\,M_\odot\,\mathrm{pc}^{-2}$ as suggested by Kennicutt (1989). For the gas density exponent k, a value of 1.5 has been assumed by Chiappini et al. (1997) in order to ensure a good fit to the observational constraints of a large set of local spirals (Kennicutt 1998). The resultant star formation history is shown in Fig. 1(a) for a 2 Kpc wide ring located 8 Kpc from the Galactic Centre, which represents the solar neighbourhood.

The IMF adopted is a simplified two-slope approximation to the actual Scalo (1986) IMF, which is expressed by the formula:

$$\phi_{\mathrm{scalo}}(m) = \begin{cases} 0.19 \times m^{-1.35} & \text{if } m < 2\,M_\odot \\ 0.24 \times m^{-1.70} & \text{if } m > 2\,M_\odot. \end{cases} \quad (2)$$

2.1.2 Ellipticals

There is a long-lasting debate on the scenario for the formation of elliptical galaxies. While it is clear that dark matter structures build up in a hierarchical fashion, with smaller structures forming first, there are strong hints that the much more complex physics of visible matter, impossible to simulate from first principles, reverses, to some extent, this trend. Indeed, recent observations (Cowie et al. 1996; Guzman et al. 1997; Brinchmann & Ellis 2000; Kodama et al. 2004; Bell et al. 2005; Juneau et al. 2005; Noeske et al. 2007) add further support to previous suggestions coming mostly from detailed studies of chemo-photometric properties (e.g. Thomas et al. 2005 and references therein) for so-called 'cosmic downsizing'; the idea that large elliptical galaxies formed their stars at high redshift in a huge burst of star formation, and after that evolved in an almost passive way (for a recent comprehensive review see Renzini 2006). Indeed, a few modern semi-analytic models (e.g. Granato et al. 2004; Bower et al. 2006) try to obtain, within a computation of hierarchical buildup of dark matter potential wells, a rapid and high-redshift assembly of baryons in large galaxies (which are dominated by ellipticals), in other words breaking the hierarchy of galaxy formation and mimicking the monolithic scenario to some extent (Somerville 2005). A fundamental ingredient may be a proper treatment of the active galactic nuclei (AGN) feedback, neglected in all previous computations, which could make these galactic systems passive after an early ($z > 2$) and short phase ($\sim$1 Gyr) of rapid mergers of similar subunits.

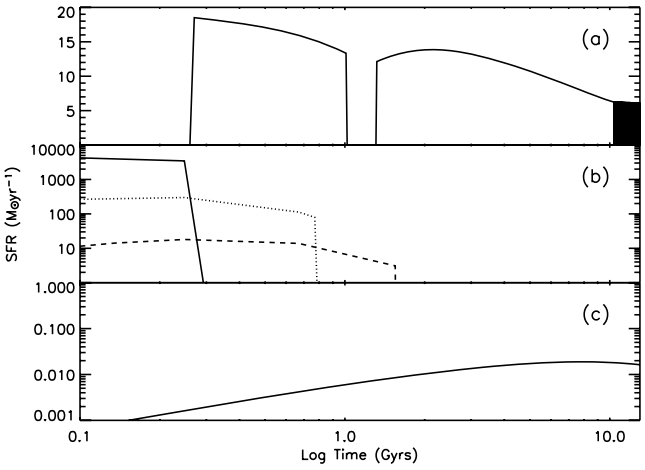

Figure 1. Predicted SF history in (a) the solar neighbourhood, (b) elliptical galaxies of masses $10^{10}\,M_\odot$ – dashed line, $10^{11}\,M_\odot$ – dotted line and $10^{12}\,M_\odot$ – solid line, (c) irregular galaxies.

A detailed modelling of the physical mechanisms responsible for the downsizing is clearly outside the scope of this paper. Thus, here we adopt and investigate the simple monolithic model proposed in CPM08 which has been carefully calibrated against the chemistry of ellipticals, deferring the investigation of alternative and more complex possibilities to future work. The elliptical galaxies in CPM08 form as a result of a rapid collapse of a homogeneous sphere of primordial gas leading to a period of intense star formation. This star formation is assumed to halt as the energy of the ISM, heated by stellar winds and SNe explosions, exceeds the binding energy of the gas, sweeping away almost all of the residual gas. At later times, the galactic wind is maintained by Type Ia SNe provided that the thermal energy exceeds that of the binding energy of the gas.

The SFR is a Schmidt law expressed as

$$\psi = \nu G^k(t), \quad (3)$$

where G is the total gas mass with an exponent $k = 1$. The star formation efficiency, ν, is assumed to increase with mass (as originally postulated in Matteucci 1994) in order to reproduce the positive correlation of [Mg/Fe] with mass (e.g. Thomas et al. 2005). In this paper, models of galaxies of three different masses have been

Downloaded from https://academic.oup.com/mnras/article/394/4/2001/1203297 by guest on 20 August 2022

followed. Galaxies with a final stellar mass of $10^{10}\,M_\odot$ (the low-mass galaxy described in CPM08) with a star formation efficiency $\nu = 5\,\mathrm{Gyr}^{-1}$. Galaxies with a final stellar mass of $10^{11}\,M_\odot$ (Model La1 as described in CPM08) with a star formation efficiency $\nu = 15\,\mathrm{Gyr}^{-1}$. Galaxies with a final stellar mass of $10^{12}\,M_\odot$ (Model Ha1 as described in CPM08) with a star formation efficiency $\nu = 25\,\mathrm{Gyr}^{-1}$. The star formation history is shown in Fig. 1(b).

The IMF adopted here is a Salpeter IMF of form:

$$\phi_{\mathrm{Salp}}(m) = 0.17 \times m^{-1.35}. \quad (4)$$

The IMF in different galactic system is a topic hotly debated in the literature. For instance, Baugh et al. (2005) showed that the only way to reproduce the statistic of submillimetre sources, usually considered the precursor of local ellipticals, in the context of their 'standard' semi-analytic model is to adopt an extremely top-heavy IMF during mergers. However, their model still shows discrepancies with observed trends of α/Fe in local ellipticals (Nagashima et al. 2005), and predicts masses of submillimetre sources too low by more than one order of magnitude (Swinbank et al. 2008).

2.1.3 Irregulars

Two separate formation scenarios for irregular galaxies were proposed in CPM08. In this paper, only the first scenario is followed, in which the irregular galaxies are assumed to assemble from the infall of protogalactic small clouds of primordial chemical composition and to produce stars at a slower rate than spirals. This formation scenario has been proposed to model dwarf irregular galaxies of a Magellanic type.

The SFR is a Schmidt law as shown in equation (3), with $k = 1$ and a low-star-formation efficiency $\nu = 0.05\,\mathrm{Gyr}^{-1}$. The star formation history is shown in Fig. 1(c). The IMF adopted is Salpeter as given by equation (4).

2.2 Dust evolution

In addition to the gas phase, the CPM08 model also follows the evolution of several of the elements in the interstellar dust. The elements considered are C, O, Si, Mg, Fe and S. The factors considered are similar to those affecting the evolution of the ISM and are:

(i) the subtraction of dust elements due to star formation.
(ii) the production in stellar winds in low- and intermediate-mass non-binary stars with masses 0.8–8 $M_\odot$.
(iii) the production in Type Ia SNe by binary stars in systems with combined masses 3–16 $M_\odot$.
(iv) the production in Type II SNe of massive stars of masses 8–100 $M_\odot$.
(v) the loss of dust in outflows due to galactic wind.
(vi) the destruction of dust primarily from SNe shocks.
(vii) the accretion of dust in dense MCs.

The dust condensation efficiencies assumed in the stellar winds and in SNe are those suggested by Dwek (1998).
The destruction rates in SNe shocks and the accretion rates in MCs follow suggestions by McKee (1989) and Dwek (1998).

2.2.1 Spirals

In the paper of CPM08, only the dust properties of the solar neighbourhood are considered.

The accretion rates are set to realistic values following Dwek (1998), and the destruction rates are set separately for each element

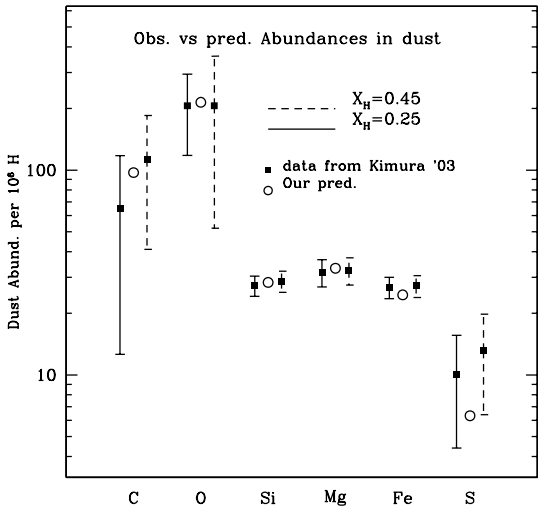

Figure 2. Comparison between the predicted dust abundances for the refractory elements by the CPM08 model for the solar neighbourhood (circles) and the elemental abundances observed in the local interstellar cloud by Kimura, Mann & Jessberger (2003) (squares), using two different estimates of the ionization fraction of hydrogen.

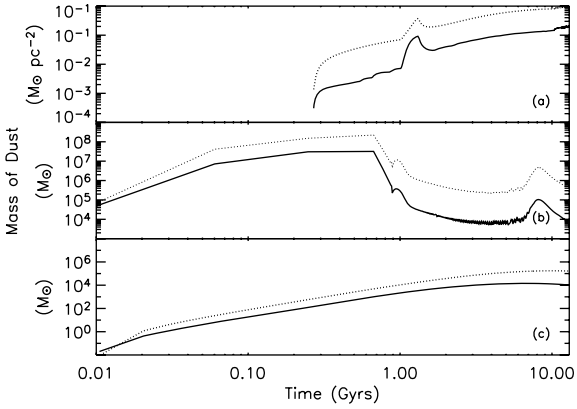

Figure 3. Predicted evolution of the dust masses for galaxies of different morphologies, showing evolution of carbon (solid line) and silicates (dashed line); (a) spiral galaxies; (b) elliptical galaxies and (c) irregular galaxies.

and are related to their individual condensation temperatures, so that depletion fractions of the elements in the model can reproduce those observed in the local warm medium. The results are shown in Fig. 2. For the purposes of this paper, we are interested in following the evolution of the mass of carbon dust particles and silicates (dust particles composed of O, Mg, Si, S, Ca, Fe). The evolution of these particles is shown in Fig. 3(a).

The solar neighbourhood is believed to be representative of the Galaxy as a whole. Hence, for this paper, the properties calculated for the solar neighbourhood will be used as global properties for the whole galaxy.

2.2.2 Ellipticals

For the initial starburst phase, the same efficiencies for accretion and destruction as in the solar neighbourhood are assumed. However, after the onset of the galactic winds elliptical galaxies will be largely devoid of cold gas. Therefore, it is assumed that no accretion

Downloaded from https://academic.oup.com/mnras/article/394/4/2001/1203297 by guest on 20 August 2022

can occur, and a much lower value for the destruction efficiency is used, as derived by McKee (1989), for a hot and rarefied medium. Also, an additional destruction term is included to treat the thermal sputtering which is thought to be the dominant source of destruction in hot plasmas. Following Itoh (1989), we assume that in an $\sim$1 keV plasma nearly 90 per cent of the dust grains will evaporate by sputtering in $\tau_{\mathrm{destr_{sput,i}}} \sim 10^5/n_{\mathrm{e}}\,(\mathrm{yr\,cm^{-3}})$, where the electron density has been self-consistently evaluated at each time-step. The resultant dust evolution is shown in Fig. 3(b).

2.2.3 *Irregulars*

For irregular galaxies, the destruction value for the solar neighbourhood is used. However, since the observed molecular H content in dwarf irregular galaxies is very small, with molecular-to-atomic gas fractions of $\sim$10 per cent or lower (Lisenfeld & Ferrara 1998; Clayton et al. 1996), it is assumed that no accretion can occur. The resultant dust evolution is shown in Fig. 3(c).

3 THE STELLAR POPULATION AND DUST MODEL

The far-UV to radio SEDs of the models, discussed in Section 2, will be calculated using the GRASIL code which follows the evolution of the stellar population, constructing a SED at any given time, first taking into account the extinction and emission by dust. All the details are given in S98, and only a summary of the main features is presented here.

Though during certain phases of galaxy evolution AGN activity may substantially contribute in shaping the observed SED of the galaxy, both providing an additional point-like source in the centre of the galaxy and contributing to the heating of galactic dust, in this paper we do not consider this complication, which we postpone to future investigation. This is justified by the fact that quasi-stellar object (QSO) lifetimes are commonly estimated to be less than 100 Myr (e.g. McLure & Dunlop 2002; Marconi et al. 2004; Shankar et al. 2005; Hopkins & Hernquist 2008), so that during the majority of the life of a galaxy any effect will be negligible.

3.1 Stellar population model

The single stellar populations included in GRASIL are based on the Padova stellar models and cover a large range in ages and metallicity. The simple stellar populations (SSPs) include asymptotic giant branch (AGB) isochrones, which incorporate a treatment of the dusty envelope around these stars, and have been calibrated on the most recent data for the V – K colours of the Large Magellanic Cloud's star clusters (see Bressan, Granato & Silva 1998; Marigo et al. 2008). The spectral synthesis technique consists in summing up the spectra of each stellar population provided by a SSP of appropriate age and metallicity (Z), weighted by the SFR (Ψ) at the time of the stars' birth (Bressan, Chiosi & Fagotto 1994):

$$F_\lambda(t_{\mathrm{G}}) = \int_0^{t_{\mathrm{G}}} \mathrm{SSP}_\lambda[t_{\mathrm{G}} - t,\, Z(t)] \times \Psi(t)\,\mathrm{d}t, \qquad (5)$$

where t_{G} is the age of the galaxy and t is the birth age of an individual SSP (see also below the treatment of age-dependent attenuation). The SFR and the metallicity values are those calculated by the chemical evolution model (see Section 2.1).

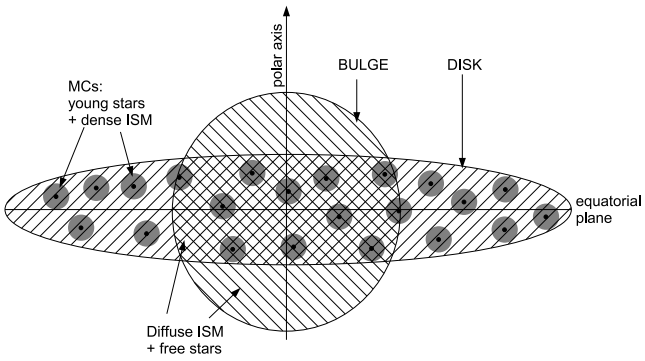

Figure 4. Sketch of geometry of stars and dust in the GRASIL model for the case of a galaxy with both a disc and a bulge.

3.2 Dust model

GRASIL then calculates the radiative transfer of the starlight, the heating of the dust grains and the emission from these grains, with a self-consistent calculation of grain temperatures, for an assumed geometrical distribution of the stars and dust and a specific grain model.

The stars can be modelled in two main components: the bulge and the disc, the latter not being present when modelling elliptical galaxies. The geometry is shown in Fig. 4. The spherical bulge has an analytic King profile, $\rho \propto (r^2 + r_c^2)^{-3/2}$, extended up until the tidal radius $r_{\mathrm{t}} = 10^{2.2}\, r_c$, where the scalelength r_c is a free parameter. The disc is described by a radially and vertically exponential profile, $\rho \propto \exp(-R/R_{\mathrm{d}})\exp(-|z|/z_{\mathrm{d}})$ truncated at $r_{\mathrm{t}} = 6R_{\mathrm{d}}$, where the radial scalelength R_{d} and vertical scalelength z_{d} are free parameters.

The dust component has the same disc and bulge profiles as the stellar component but can have scalelengths independent of the stellar component. Within these profiles, the gas and dust are further split into two main components: dense MCs and diffuse cirrus. The ratio of the total mass in dust and gas located in the MCs to the total gas mass is a free parameter f_{mc}. When a galaxy is composed of only a bulge or a disc, the MCs are dispersed evenly throughout the galaxy; however when a galaxy is modelled with both a disc and a bulge, as shown in Fig. 4, the MCs are located solely in the disc. Stars are assumed to form inside the MCs and progressively escape them on a time-scale t_{esc}. Specifically, the fraction of stars inside clouds at time t after they formed is assumed to be

$$F(t) = \begin{cases} 1 & (t < t_{\mathrm{esc}}) \\ 2 - \frac{t}{t_{\mathrm{esc}}} & (t_{\mathrm{esc}} < t < 2t_{\mathrm{esc}}) \\ 0 & (t > 2t_{\mathrm{esc}}), \end{cases} \qquad (6)$$

where t_{esc} is a free parameter of the model. The radii and mass of the MCs are also free parameters of GRASIL, though the results actually depend only on the combination $M_{\mathrm{mc}}/R_{\mathrm{mc}}^2$ which determines together with the dust-to-gas ratio the optical depth of the clouds (see S98), where M_{mc} is the mass of a MC and R_{mc} is the radius of a MC.

The dust is assumed to consist of a mixture of carbonaceous and silicate grains and polycyclic aromatic hydrocarbons (PAHs). The carbonaceous particles are assumed to have the optical properties of randomly orientated graphite spheres. The silicate grains are assumed to be amorphous silicates. The optical properties of silicate and graphite grains are taken from Laor & Draine (1993) and the optical properties of PAH molecules from Draine & Li (2007). The size distribution used in this paper for our fiducial models is those chosen by S98 to match the extinction and emissivity curves

Downloaded from https://academic.oup.com/mnras/article/394/4/2001/1203297 by guest on 20 August 2022

Table 1. Parameters for size distribution of the dust component in different environments (see equation 7). The MW size distribution is that derived by S98 to match observations from the MW. The SMC and QSO SDSS J1048+46 size distributions are calculated in this paper to match observed extinction curves.

	MW (S98)	SMC	QSO SDSSJ 1048+46
Carbon			
$a_{\rm min}$ (Å)	8	5	...
a_b(Å)	50	25	400
$a_{\rm max}$(Å)	2500	1000	700
β_1	−3.5	−3.0	−3.5
β_2	−4.0	−4.5	...
Silicate			
$a_{\rm min}$(Å)	...	...	...
a_b(Å)	50	50	5
$a_{\rm max}$(Å)	2500	10000	10000
β_1	−3.5	−3.9	−3.5
β_2	...	...	...

of the local ISM. The size distribution for both the carbon and silicate components is described by a double power law specified by equation (7):

$$\frac{{\rm d}n_i}{{\rm d}a} = \begin{cases} A_i n_{\rm H} a^{\beta_1} & a_b < a < a_{\rm max} \\ A_i n_{\rm H} a^{\beta_1-\beta_2} & a_{\rm min} < a < a_b \end{cases}, \quad (7)$$

where ${\rm d}n_i$ is the number density of grains of type 'i' with radii in the interval $[a, a + {\rm d}a]$, $n_{\rm H}$ is the number density of H nuclei and A_i is the atomic abundance of type 'i' relative to hydrogen. The size ranges ($a_{\rm min}$), (a_b) and ($a_{\rm max}$) of the dust grains and the exponents β_1 and β_2 are free parameters with values shown in Table 1. In this work, the total mass of dust and also the fraction of the graphite component to the silicate one are those calculated by the CPM08 chemical evolution model.

The luminosities of the different stellar components (the stars in the bulge, in the disc and young stars still in clouds) are calculated using the described population synthesis model. The GRASIL code then calculates the radiative transfer of the starlight through the specified dust distribution. For the MCs, a full radiative transfer calculation is performed; however for the diffuse dust the effects of scattering are only approximated by assuming an effective optical depth related to the true absorption and scattering optical depths by $\tau_{\rm eff} = [\tau_{\rm abs}(\tau_{\rm abs} + \tau_{\rm sca})]^{1/2}$. The dust-attenuated stellar radiation field can be calculated at any point inside of outside the galaxy. Then GRASIL calculates for each point in the galaxy the adsorption of radiation, thermal balance if in thermal equilibrium or thermal fluctuations if not, and reemission for each grain composition and size. Combining the contributions from the attenuated starlight and from the dust re-emission, a SED for the galaxy is calculated which depends on the angle the galaxy is viewed from.

3.3 Choice of parameters

The value of the GRASIL parameters chosen for the different galaxies is listed in Table 2. The reasons for the choices made are given below.

3.3.1 Escape time-scale ($t_{\rm esc}$)

This is a very important parameter controlling how long the young stars remain in their birth clouds. A value of 2 Myr for spiral and irregular galaxies is chosen following Granato et al. (2000). S98 found that larger values were needed to fit local starbursts, $t_{\rm esc} = 20$–60 Myr, to reflect the dense dusty environments found. In a similar way, one would expect much higher escape time-scales for the early starbursting phase of elliptical galaxies. The rates of star formation, however, predicted by the CPM08 model far exceed those observed in local starbursting galaxies, and as a result the escape time-scale could reasonably be expected to still be longer. This value remains a free parameter of the model since the precise dust condition present in SCUBA galaxies is unknown. In this work, it has been set to 250 Myr, a value found to provide good fit to SCUBA galaxies at high redshift (see Section 5.3.1). After the onset of the galactic winds in the elliptical galaxy, all of the cold gas is blown out of the galaxy, and MCs cannot form; as a result star formation is stopped and consequently $t_{\rm esc} = 0$.

Table 2. Adopted values for the GRASIL parameters – for the elliptical models, the values outside the brackets are for the starbursting phase and the values in the brackets are for the passively evolving phase.

	Spiral	Elliptical		Irregular
		10^{11} M$_\odot$	10^{12} M$_\odot$	
$t_{\rm esc}$[1]	2	250 (0)	250 (0)	2
$f_{\rm mc}$[2]	0.5	0.5 (0)	0.5 (0)	0.1
r_c^{*}[3]	...	0.21 (0.21)	0.68 (0.68)	...
$r_{\rm d}^{*}$[4]	2.35	... (...)	... (...)	1
$z_{\rm d}^{*}$[5]	0.14	... (...)	... (...)	0.5
r_c^{d}[6]	...	0.21 (0.42)	0.68 (1.36)	...
$r^{d}{}_{\rm d}$[7]	5	... (...)	... (...)	1
$z^{d}{}_{\rm d}$[8]	0.1	... (...)	... (...)	0.5
$M_{\rm mc}$[9]	10^6	10^6 (10^6)	10^6 (10^6)	10^6
$R_{\rm mc}$[10]	16	16 (16)	16 (16)	40

[1]Time-scale for the evaporation of MCs (in Myr).
[2]Fractionary gas content in the MCs.
[3]Radial scalelength of the stellar component in the bulge (in Kpc).
[4]Radial scalelength of the stellar component in the disc (in Kpc).
[5]Vertical scalelength of the dust component in the disc (in Kpc).
[6]Radial scalelength of the dust component in the bulge (in Kpc).
[7]Radial scalelength of the dust component in the disc (in Kpc).
[8]Vertical scalelength of the dust component in the disc (in Kpc).
[9]Total gas mass in each Mc (in M$_\odot$).
[10]Radius of each MC (in pc).

3.3.2 Optical depth of MCs ($M_{\rm mc}$, $R_{\rm mc}$)

Combined, these two parameters control the optical depth of the MCs, according to the ratio $M_{\rm mc}/R_{\rm mc}^2$, where $M_{\rm mc}$ is the mass of a MC and $R_{\rm mc}$ is the radius of a MC. Following Granato et al. (2000), values of $M_{\rm mc} = 10^6$ M$_\odot$ and $R_{\rm mc} = 16$ pc are chosen for the spiral and elliptical galaxies, values which have been found to give good SED fits and are consistent with observations.

GRASIL has not been previously used to model irregular galaxies. In order to fit the SED in the mid-infrared (MIR), MCs with a lower optical depth had to be used in this work (see Section 5).

3.3.3 Ratio of gas mass in MCs to total gas mass ($f_{\rm mc}$)

For spiral galaxies, we choose a value of $f_{\rm mc} = 0.5$ for this parameter which agrees well with the values used to fit local spirals in S98.

Downloaded from https://academic.oup.com/mnras/article/394/4/2001/1203297 by guest on 20 August 2022

The passively evolving late phase in elliptical galaxies will have no MCs, so $f_{\rm mc} = 0$. A value of 0.5 is adopted for the starbursting stage.

Lower value for the molecular-to-atomic gas fraction is observed in irregular galaxies than in spiral galaxies (see Section 2.2.3); and since most of the hydrogen in MCs is in H_2, while most of the diffuse cirrus gas will be atomic H_1 this lower value suggests a lower value of $f_{\rm mc}$. Consequently, a value of $f_{\rm mc} = 0.1$ has been chosen.

3.3.4 Geometry (r_c^*, $r_{\rm d}^*$, $z_{\rm d}^*$, r_c^d, $r_{\rm d}^d$, $z_{\rm d}^d$)

The spiral galaxy is modelled as a pure disc for both the stellar and the dust components with scalelengths ($r_{\rm d}^*$ and $z_{\rm d}^*$ for the stellar component and $r^d{}_{\rm d}$ and $z^d{}_{\rm d}$ for the dust component) set following the results of Misiriotis et al. (2006), who used *COBE*/Diffuse Infrared Background Experiment maps and *COBE*/Far Infrared Absolute Spectrophotometer spectra to constrain a model for the spatial distribution of the dust, the stars and the gas in the Milky Way.

The elliptical galaxies are modelled using a pure bulge for both the stellar and the dust components. The elliptical stellar scalelength, r_c^*, is given by the chemical evolution model of CPM08. S98 found that in order to obtain a good fit to a template constructed from local elliptical galaxies a dust scalelength, r_c^d, much larger than the stellar scalelength was required. This conclusion was also reached by Panuzzo et al. (2007) who found it necessary to have dust scalelengths almost double the stellar ones in order to fit a late-type galaxy of the Virgo cluster. Spatially extended dust has also been observationally detected by Temi, Brighenti & Mathews (2007), who have detected spatially extended dust in two optically normal galaxies, NGC 5044 and NGC 4636. Although it should be noted that Temi et al. (2007) concluded that due to the short sputtering lifetime for extended dust $\sim$7 Gyr and no evidence for a recent merger that the most likely source of this dust was due to galactic winds powered by a central AGN, whereas in the CPM08 model the proposed mechanism for the galactic wind is different, with SN1a and stars alone able to power the wind for several Gyr (see Pipino et al. 2005). Therefore, due to observational evidence and also typical values used in previous studies, in the passively evolving phase, we have set the dust scalelength to be twice the stellar scalelength. For the early starbursting phase, the dust is likely to be more concentrated, so the dust scalelength is set equal to the stellar one.

The irregular galaxy is modelled as a pure disc for both the stellar and the dust components. Observations for the dust distribution in irregular galaxies are still largely inconclusive, so we have set the dust scalelength equal to the stellar one.

3.4 Generating SEDs

In order for GRASIL to be able to calculate the intrinsic stellar SED of a galaxy, the stellar population code requires a star formation history and a metallicity evolution which are generated by the chemical evolution code, and an IMF which is set to that used in the chemical evolution code. To calculate the dust-effected SED, GRASIL requires a total mass in dust (in this work the dust-to-gas ratio will be the quantity discussed) and chemical composition of dust (the carbon-over-silicate ratio) which are set by the dust evolution model; the other geometrical parameters are then set to the values described in Section 3.3, and the grain size distribution to that derived in S98.

For comparison, SEDs are also calculated for galaxies with the chemical evolution described by the CPM08 model but without the detailed dust evolution properties. Instead, two common assumptions will be adopted.

(i) That the ratio of the dust-to-gas mass is proportional to the metallicity, through a constant normalized to the Milky Way, using the value 0.008 calculated from observations for the dust-to-gas mass ratio as discussed in CPM08. So, *dust mass* $\propto$ *metallicity*$\times$ *gas mass*.

(ii) That the chemical composition does not evolve. So that the fraction of carbon to silicate will be set to the value 0.19 for all times and morphologies, a theoretical value found by CPM08 for the ratio of C/Si at 13 Gyr in the solar neighbourhood model.

In addition, for the irregular galaxy and for the starbursting phase in elliptical galaxies, the effect on the SED of releasing a third assumption, made routinely in other works as well as for the fiducial models in this paper, namely that the dust size grain distribution does not evolve and remains constantly identical to that of the Milky Way, is investigated.

For clarity, when the full dust treatment is used as described in the CPM08 paper, it will be referred to as the full CPM08 model. When the two assumptions outlined above are adopted, it will be referred to as the simple dust model. The difference between the two models will be referred to as the *disparity*. This would be the error introduced by the adoption of the simplifications if one assumes that the fiducial model is correct. It is only a theoretical error.

3.5 Treatment of PAH molecules

The abundance of PAHs is calculated from the chemical composition of the dust predicted by the CPM08 model, specifically their abundance is proportional to the total abundance of carbon molecules in the dusty component of the ISM. The exact treatment of the absorption and emission processes for the PAH bands is then calculated following the same procedure described in S98 and Vega et al. (2005) but updated with the most up-to-date cross-sections outlined in Draine & Li (2007) calculated using new laboratory data and spectroscopic data observed by the *Spitzer Space Telescope.*

Although PAH emissions have been found to be a ubiquitous feature of both the Milky Way and external galaxies, it is worth noting that the strengths of the PAH bands have been found to vary between galaxies, with low-metallicity galaxies and galaxies hosting AGN in particular being found to be deficient in PAH emission. This has led several authors to speculate that the abundances of PAHs could be linked to the particular environmental conditions present in their host galaxy. For example, it is thought that they could be preferentially destroyed by strong UV radiation (e.g. Madden et al. 2006), and could be more susceptible to SNe shocks (e.g. O'Halloran, Satyapal & Dudik 2006). This suggests that the evolution of PAHs may not necessarily be identical to that of the larger carbon grains. This effect has been partly accounted for by following the treatment of PAHs outlined in Vega et al. (2005). Where in order to agree with observations from around hot stars and HII regions, from within our galaxy, the abundance of PAHs in the MCs within GRASIL, where the UV radiation will be strongest, had to be suppressed by a large factor ($\approx$1000 with respect to the cirrus component). Using such a prescription, it was shown that GRASIL could reproduce the MIR spectrum of local star-forming galaxies.

Since in this work the evolution of the PAH dust population has not been specifically followed, a detailed analysis of the spectrum in the MIR will not be possible. However, linking the abundance of the PAHs to both the environment, by suppressing the PAH abundance in MCs, and to the chemical composition of the dust should be a

Downloaded from https://academic.oup.com/mnras/article/394/4/2001/1203297 by guest on 20 August 2022

reasonable approximation and be sufficient to highlight broad trends in the emission from this region.

3.6 Comparison to observations

3.6.1 Low redshift

The theoretical SEDs are compared to observed nearby galaxies of similar morphological type. The data sample used is that described in Dale et al. (2007) which presents SEDs for the 75 galaxies of the Spitzer Infrared Nearby Galaxies Survey (SINGS) sample selected to span a wide range of morphologies, luminosities and IR to optical ratios. The data set comprises galaxies at an average distance of $\sim$10 Mpc and contains SEDs from UV to radio wavelengths and includes the following.

(i) UV data from Galaxy Evolution Explorer (GALEX).

(ii) Optical fluxes from the Third Reference Catalogue of Bright Galaxies (RC3) catalogue (de Vaucouleurs et al. 1991).

(iii) IR data from Two-Micron All-Sky Survey, *ISO*, *IRAS*, *Spitzer.*

(iv) Submillimetre data from SCUBA.

(v) Radio data from the literature including the New Very Large Array Sky survey.

All the galaxies of a particular morphological type are normalized to a common value in the *K* band.

Our spiral model is designed to reproduce observations of the Milky Way, hence, to represent this morphological type, all spirals of type SBb to SBc and SAb to SAc in the SINGs data set were chosen, numbering 24. Our irregular galaxy is designed to reproduce observables of Magellanic-type irregular galaxies, therefore the 10 galaxies of type Im will be used. Our elliptical galaxy model is designed to reproduce the observables of passively evolving elliptical galaxies. Of the six elliptical galaxies in the SINGS sample, two galaxies, NGC 855 and NGC 3265, show very bright UV colours in addition to strong IR emission probably indicating ongoing moderate star formation. These two galaxies were identified as star-forming galaxies by Dale et al. (2007) and were therefore not used in this work.

3.6.2 High redshift

In order for the elliptical galaxy formation scenario presented in this work to be correct, one would expect to find observed galaxies at high redshift with SEDs similar to those presented in this work. It is therefore essential to check that our young elliptical models are representative of the birth of typical elliptical galaxies at high redshift, by comparing the theoretical models to observations. However, for each of the masses of galaxy, only one star formation history has been followed with a fixed set of values for all of the parameters, so the models could not be expected to account for all high-redshift objects. Also, due to the sheer variability of high-redshift galaxies the construction of an 'average' high-redshift SED is not possible. Consequentially, we compare our models to two different high-redshift data sets (details of which can be found in the relevant sections), each thought to be a representative of a different stage of the young galaxies evolution, to check that a reasonable proportion of the observed galaxies have SEDs similar to that predicted by our models.

A chi-squared fitting technique was employed to calculate the age and redshift of the model which gives the best fit to the observed points. Theoretical SEDs for the elliptical galaxy in its starbursting and post-starbursting phases were generated at several time-steps, from 0.05 to 2 Gyr. Each of these SEDs is then normalized and compared to the observed spectra of the galaxy. Since neither of the data sets has spectroscopic redshifts, the theoretical SEDs at all the time-steps are compared to the observed SED for a range of redshift values, and then the age and redshift which correspond to the best fit are selected using a chi-squared minimization technique. Due to the inherent uncertainty from using such a limited template set, in order to avoid spurious results the possible redshift range will be limited to within 30 per cent of the photometric redshift values calculated previously by other authors, using more sophisticated fitting procedures.

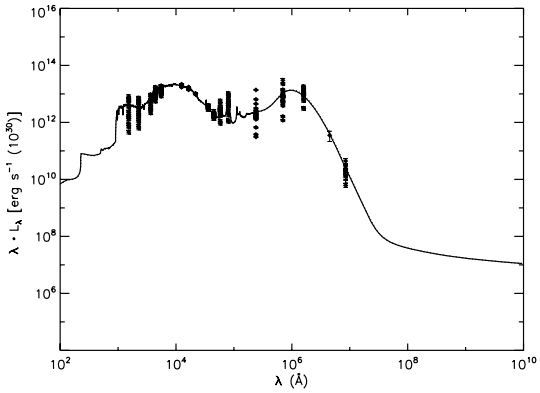

Figure 5. Comparison of theoretical spiral model at 12 Gyr with the SEDs from all spiral galaxies of morphological type ranging from SBb to SBc and SAb to SAc in the SINGS sample, normalized to the *k* band. Solid line – full CPM08 model. Dotted line – simple dust model.

4 RESULTS

4.1 Properties of spiral galaxies

Fig. 5 shows the results for the theoretical SEDs generated at 12 Gyr compared to the mean SED of spiral galaxies of types SBb to SBc and SAb to SAc from the SINGS sample. The theoretical model shows a good correlation with the observed spiral galaxies. This suggests that the assumption that the global properties of the galaxy can be represented by the chemical and dust evolution model of the solar neighbourhood at late times is a good one.

The evolution of the SED of spiral galaxies is shown in Fig. 6. Due to the mainly quiescent slow evolution of the spiral galaxies, the SEDs do not show large changes throughout their lifetime, and there is little variation in the percentage of starlight reprocessed by the galaxy which for ages greater than 1 Gyr remains fairly constant at a value of 30 per cent (see Fig. 7).

Also included in Fig. 6 are the SEDs generated for the same chemical evolution model but adopting the two dust assumptions. Since the simple dust assumptions are normalized to the full CPM08 model for the solar neighbourhood at 13 Gyr, the SEDs at 12 Gyr are still in very close agreement. As the age of the galaxy decreases, the residuals increase as the assumptions made for the dust-to-gas ratio and carbon over silicate ratios diverge from our theoretically calculated values (Fig. 8).

Of the two simplifications, the disparity introduced by assuming a dust-to-gas ratio dominate the residuals. Assuming a constant Milky Way chemical composition of the dust has little effect on the SED because after initial fluctuations during the first 2 Gyr this ratio remains fairly constant, throughout the rest of its lifetime (Fig. 8a).

Downloaded from https://academic.oup.com/mnras/article/394/4/2001/1203297 by guest on 20 August 2022

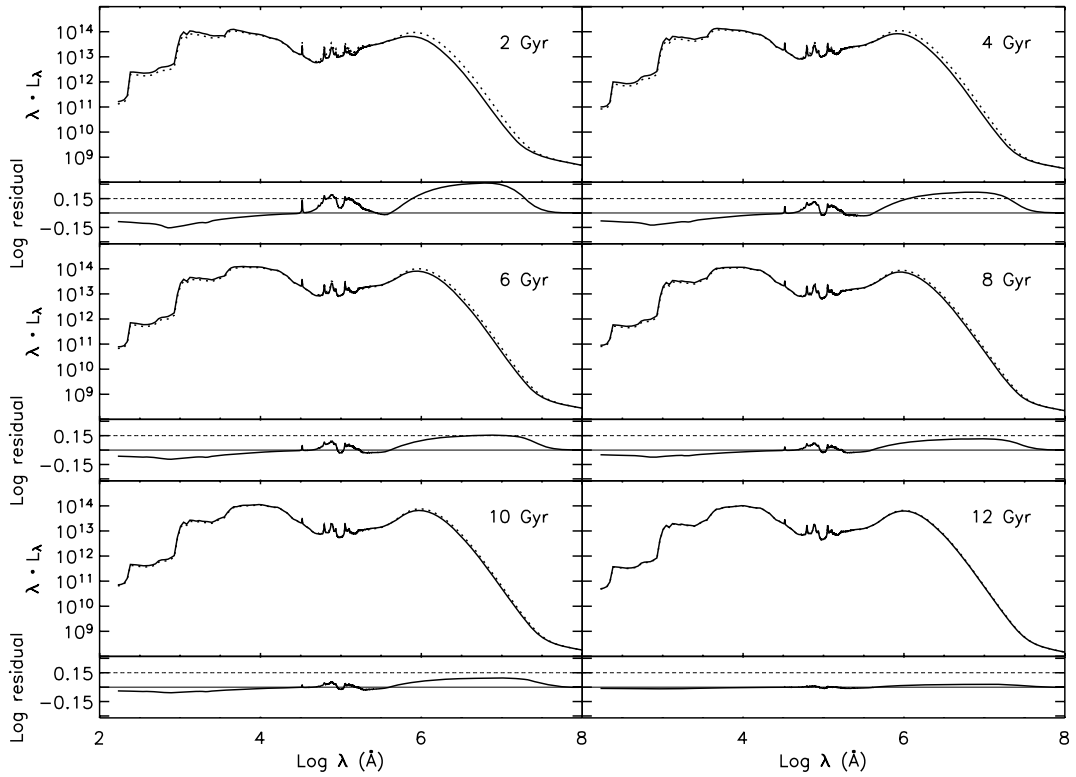

Figure 6. The evolution of the SED of the spiral galaxy. The larger six plots show the SEDs at different times in the evolution of the galaxy [with units erg s^{-1} (10^{30})]. The solid line shows the SEDs generated using the full CPM08 model, the dashed line shows the evolution adopting the simple dust model. The lower panels display the log residual between the two models.

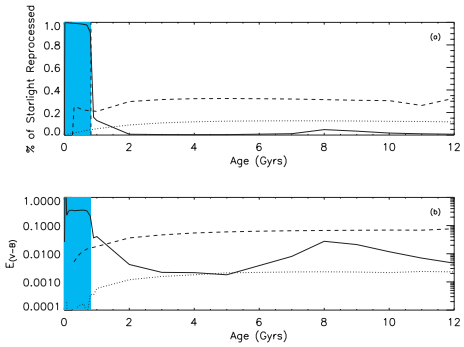

Figure 7. (a) Fraction of stellar radiation dust reprocessed: solid line – elliptical; dotted line – irregular; dashed line – spiral. (b) Evolution of extinction coefficient: solid line – elliptical; dotted line – irregular; dashed line – spiral. The blue shaded area represents the age before the galactic wind starts in the elliptical model during which it is undergoing a period of extreme star formation.

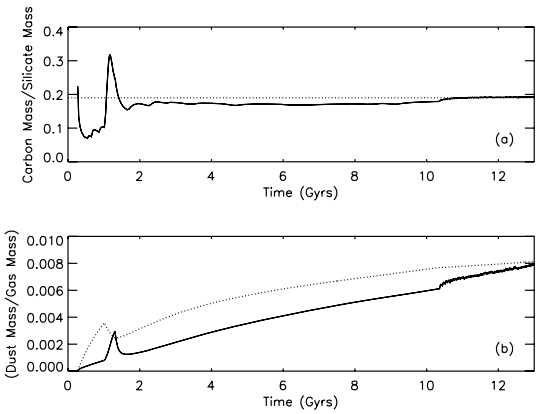

Figure 8. Spiral galaxy. (a) Comparison between the value of the C/Si calculated by the full CPM08 ratio (solid line) with the constant value assumed if the chemical abundance remains identical to the present value for the solar neighbourhood (dotted line). (b) Comparison of the dust-to-gas ratio value calculated by the full CPM08 model (solid line) with the expected value if a dependence on the metallicity is assumed (dotted line).

Hence, making the simplification that the chemical composition does not evolve with time will only lead to small differences in the SED (Fig. 9a) for the majority of the spiral galaxies life. At early times, the different chemical composition calculated mainly affects the MIR part of the SED due to the resulting differences in the abundance of PAHs.

The assumed dust-to-gas ratio, however, leads to a more significant disparity particularly when the galaxy is younger (Fig. 9b), since our model predicts a relationship between the dust-to-gas ratio and the metallicity which is not entirely linear (Fig. 8b). Therefore, adopting this assumption will introduce disparities which largely increase as the age of the galaxy decreases. This assumption will result in too much dust in the galaxy, and this will lead to an excess of reprocessing. The disparity will be most significant in the FIR part of the spectrum (Fig. 9b).

In this paper, only the chemical evolution in the solar neighbourhood has been followed, and the SED of the whole galaxy has been constructed by globalizing the results. Although this has been shown to be a reasonable assumption for old spiral galaxies in the

Downloaded from https://academic.oup.com/mnras/article/394/4/2001/1203297 by guest on 20 August 2022

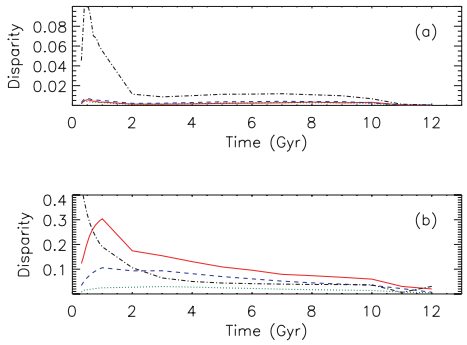

Figure 9. The residuals between the SEDs generated by the full spiral CPM08 model and SEDs generated by using the simplifications that (a) the chemical composition remains equal to the Milky Way values at all times, (b) the dust-to-gas ratio scales with the metallicity. Blue dashed line – UV, green dotted line – optical/NIR, black dot/dashed line MIR, red solid line – FIR. The disparity is given as the absolute mean log value of the residuals between the two models in the specified wavelength region.

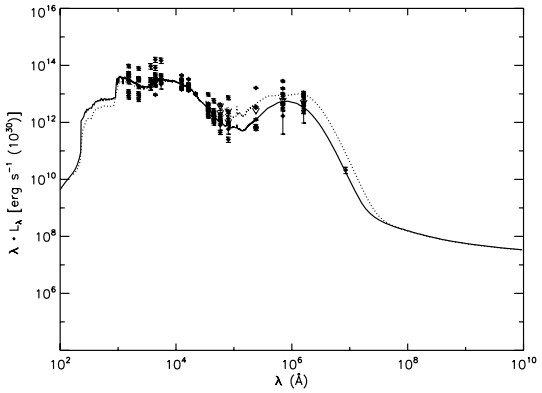

Figure 10. Comparison of theoretical irregular model at 12 Gyr with SEDs of all irregular galaxies of Magellanic type in the SINGS sample. Solid line – full CPM08 model. Dotted line – simple dust model.

local universe, since the SEDs generated are representative of observations, it is unlikely to be valid at higher redshifts. The chemical evolution has two infall episodes: first, the halo and the thick disc form followed by the second phase in which the thin disc forms. So at early times, the halo and thick disc will dominate the galaxy properties and the global properties could differ greatly from that of the solar neighbourhood. The results for spiral for very young galaxies (ages $\leq$1 Gyr) should therefore be taken with caution.

The CPM08 model and indeed all complete dust evolution models currently written only deal with the total mass of different elements contained in grains. As a result, no information is contained regarding how these elements are combined to form grains and what size distribution these grains should have. Instead a composition and size distribution for the dust grains must be assumed. In previous works using GRASIL, it has been usual to use the grain distribution population suggested in S98. In that paper, both the observed extinction curves from the diffuse medium within the Milky Way and the observed galactic emission from dust were reproduced using a combination of graphite and silicate grains and PAH molecules.

Our spiral chemical and dust evolution model is designed to match observed properties of the solar neighbourhood, and as a result it should also be capable of reproducing the observed galactic extinction and emission. Our model, however, predicts a slightly different ratio for the dust-to-gas ratio as well as a different graphite-to-silicate ratio than that used in S98. Therefore, if we use the S98 size distribution in combination with the theoretical quantities of dust, we have calculated the resultant extinction and emission properties will differ slightly from those observed.

No adequate dust model was found in the literature which could satisfactorily reproduce the observed extinction curves with the low value of 0.19 for the ratio of carbon to silicon predicted by our model (e.g. see Zubko et al. 2004). Hence, for simplicity, the S98 dust composition already included within the GRASIL model was used. A likely possibility is that existing dust models are tuned on low-density environments (cirrus), while our C/Si value should refer to a galactic average.

4.2 Properties of irregular galaxies

Fig. 10 shows the results for the theoretical SEDs generated at 12 Gyr compared to the SEDs for all the Magellanic-type irregular galaxies of the SINGS sample. Although the irregular galaxies show some scatter in their SEDs, the theoretical model manages to fit the average properties remarkably well. Also shown in the figure is the generated SED if the two dust simplifications are used. By using these simplifications, quite a clear discrepancy between the two SEDs is introduced particularly in the IR and UV. Although still largely consistent with the observed SEDs, there is a strong hint that the simplified dust treatment is leading to more dust reprocessing than that observed in the average galaxy in the sample. A common measure of the quantity of dust reprocessing in a galaxy is the observed IR/UV ratio (e.g. Dale et al. 2007). Using the same formalism as Dale et al. (2007) and equation (4) from Dale & Helou (2002), the median total IR-to-UV ratio was calculated for the irregular Magellanic galaxies in the sample to be 0.22. This agrees well with the value of 0.21 calculated from the results of the full CPM08 model. For the simple dust model, however, a value of 0.67 was calculated implying that too much energy has been absorbed in the UV and emitted in the IR.

For the most part the disparity between the SED generated using the full dust treatment and that generated using the simplifications can be attributed to the assumption that the dust-to-gas ratio scales with metallicity (Fig. 11b). As Fig. 12(b) shows, the theoretical values calculated by our model are much lower than those calculated from the Milky Way scaling relation, by approximately a factor of 6. This much lower dust-to-gas ratio can be mainly attributed to the absence of accretion in our irregular galaxy model which will result in smaller quantities of dust forming than would be expected following the common Milky Way metallicity scaling relation, where dust accretion is prevalent. Such a finding is consistent with the work of Galliano et al. (2003, 2005) where dust masses were estimated for four local dwarf galaxies and for two (NGC 1569 and He 2-10), values for the dust-to-gas ratio lower by factors of 4–7 and 2–10 than expected were found and Hunt et al. (2005) and Walter et al. (2007) who estimated the dust masses in local dwarf galaxies and found values consistently smaller than expected.

Fig. 12(a) shows that at ages greater than about 2 Gyr the chemical composition calculated by the CPM08 model is significantly different from that calculated for the solar neighbourhood, resulting in a much lower C/Si ratio. Fig. 11(a) shows that the main effect on the SED of the galaxy of this lower C/Si ratio will be in the MIR part of the spectra, with only a small effect at other wavelengths. The effect on the MIR of a change in the chemical composition needs to be treated with caution, since a major contributor to this part of the spectra is PAHs, whose evolution is not specifically followed

Downloaded from https://academic.oup.com/mnras/article/394/4/2001/1203297 by guest on 20 August 2022

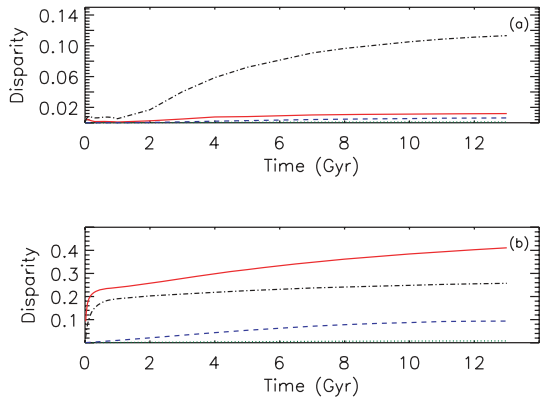

Figure 11. The residuals between the SEDs generated by the full irregular CPM08 model and SEDs generated by using the simplifications that (a) the chemical composition remains equal to the Milky Way values at all times, (b) the dust-to-gas ratio scales with the metallicity. Lines same as in Fig. 9.

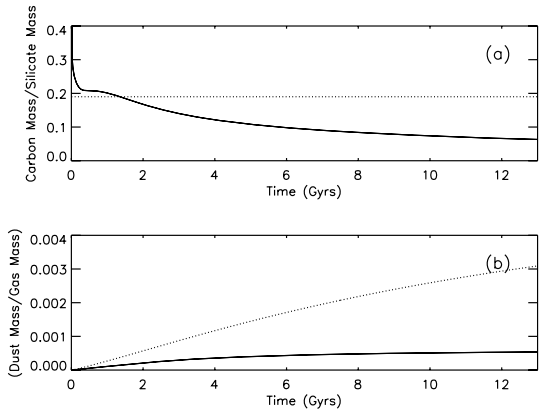

Figure 12. Irregular galaxy: (a) comparison between the value of the C/Si calculated by the full CPM08 ratio (solid line) with the constant value assumed if the chemical abundance remains identical to the present value for the solar neighbourhood (dotted line). (b) Comparison of the dust-to-gas ratio value calculated by the full CPM08 model (solid line) with the expected value if a dependence on the metallicity is assumed (dotted line).

by the CPM08 models (see Section 4.2). The effect of the lower C/Si value predicted by CPM08 on the SED will largely be due to a reduction in the number of PAH molecules and therefore in the luminosity radiated in the PAH bands.

Although the treatment of the PAHs in this work is insufficient to put any strong constraint on the nature of the PAHs in the galaxies modelled, it is worth noting the relatively low abundance of C/Si predicted for the irregular galaxy as compared to that of the solar neighbourhood. This is interesting since it is in agreement with the striking observed correlation between the strength of PAH features and the metallicity of the galaxy (see e.g. Engelbracht et al. 2005; Madden et al. 2006; Wu et al. 2006; O06), with low-metallicity galaxies, such as our theoretically modelled irregular galaxy, exhibiting very weak or no features. Several different explanations have been proposed for this correlation. These include the suggestion of more efficient PAH destructive mechanisms in lower metallicity galaxies (e.g. Galliano et al. 2005; Madden et al. 2006) due to harder radiation and the paucity of dust. Alternatively, O'Halloran et al. (2006) proposed that the PAHs could be destroyed by numerous shocks observed in low-metallicity systems. While it has also been shown by Galliano, Dwek & Chanial (2008), that it is possible to explain the trend of PAH abundance with metallicity by using chemical evolution models. Starting from the summations that lower metallicity galaxies are on average younger than higher metallicity galaxies and that carbon dust and PAHs are predominantly produced in AGB stars which recycle their ejecta into the ISM after a relatively long period of time, it follows that the trend can be seen as a reflection of this delayed injection of carbon dust into the ISM by AGB stars, since younger systems will have had insufficient time to become enriched with PAHs. The CPM08 chemical evolution models used in this work put forward a new suggestion since they show that even in older low-metallicity systems there is likely to be a lower abundance of carbon and therefore PAH molecules, a possibility which could explain or at least contribute to the observed trend.

The relatively lower value of C/Si predicted by the CPM08 model with respect to that predicted for the solar neighbourhood can be explained by examining the different production and destruction rates used in the two different environments. In the solar neighbourhood model, carbon is assumed to be destroyed with a higher efficiency than the silicates. This was chosen in order to explain the local dust abundance pattern (see CPM08), and is consistent with the fact that carbon has a condensation temperature lower than many silicates. However, the solar neighbourhood model also includes dust accretion, whose rate is assumed to be independent of the particular element. For this reason, the abundance pattern produced by the preferential destruction of certain elements is partially smoothed out by the non-differential accretion. In the irregular model, however, where dust accretion is absent, the higher destruction rate attributed to the carbon is not compensated in the same way, giving rise to the lower C/Si value.

A possible source of error in this work is the absence of an additional 'very cold grain' (VCG) component as proposed by Galliano et al. (2003, 2005). In these papers, a population of grains at very low temperatures was introduced in order to explain an excess in the emission in the submillimetre in the observed low-metallicity galaxies. Such a component could be located at the centre of dense clouds (see e.g. Galliano et al. 2003) or in the galaxies outskirts where the radiation field is weak (see e.g. Draine et al. 2007). Galliano et al. (2003, 2005) estimated that for four low-metallicity irregular galaxies between 40 and 80 per cent of the total dust mass is in the form of VCGs. Such a dust component is not currently included in our models, and if confirmed by additional submillimetre observations, the inclusion of such a large cold dust grain population should be investigated. However, any effect is likely to be slight. For the irregular galaxies, over 80 per cent of the reprocessing is taking place within the MCs, heated by the young stars (as opposed to about 25 per cent in the spiral model). The emission of which is characterized only by the geometry and dust-to-gas ratio of the MCs and would therefore be unaffected by a population of VCGs. If a substantial proportion of the rest of the dust takes the form of VCGs, the result would be a reduction in the amount of other larger sizes of dust grain in the cirrus. In our irregular model, the cirrus component only has a small observed effect on the SED at wavelengths longer than the peak IR wavelength. Therefore any effect will be slight and will probably result in a slight decrease in emission in the very FIR with a corresponding increase in emission in the submillimetre, where VCGs emit.

The evolution of the SED of irregular galaxies is shown in Fig. 13. The quiescent low SFR leads to SEDs which evolve only slightly with time. The mass of dust present in the galaxy initially increases rapidly until a time ∼1 Gyr is reached at which point it begins

Downloaded from https://academic.oup.com/mnras/article/394/4/2001/1203297 by guest on 20 August 2022

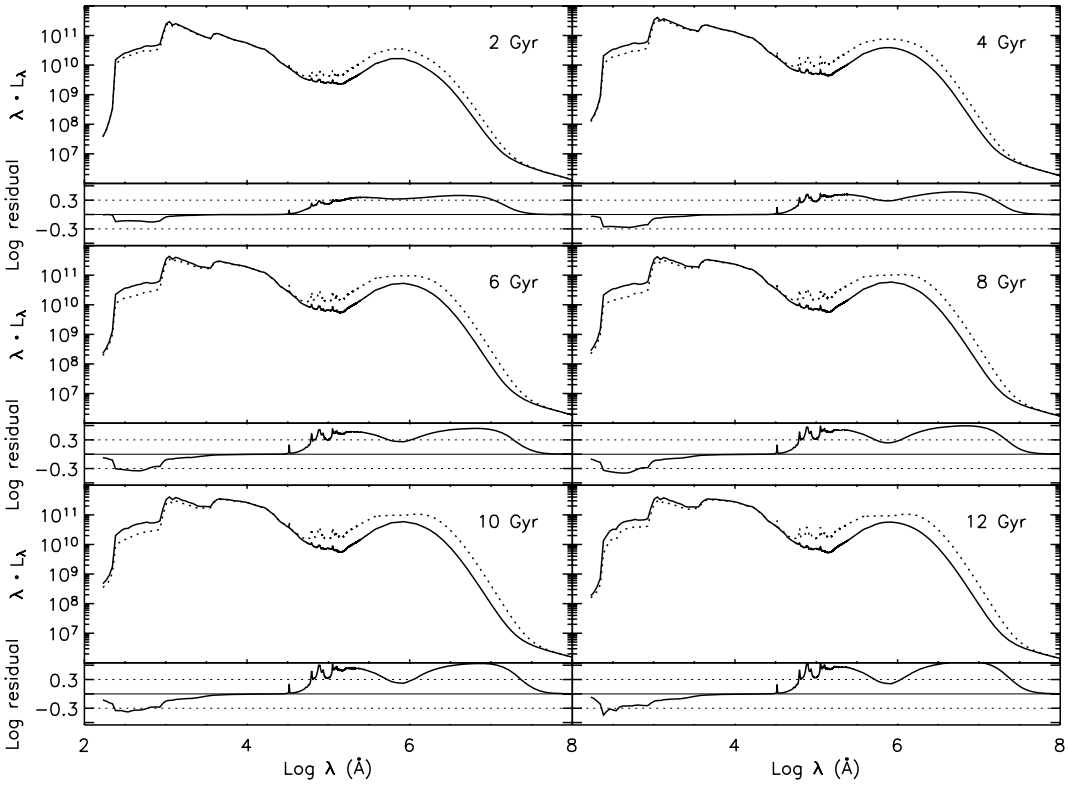

Figure 13. The evolution of the SED of the irregular galaxy, panels same as for Fig. 6.

to plateau (see Fig. 3c). The fraction of reprocessed light in the galaxy follows suit, rising rapidly to a value of ∼15 per cent and then remains fairly constant throughout its lifetime (see Fig. 7). A value which is one-half of the predicted light reprocessed in spiral galaxies.

As Fig. 11 shows the disparity between the SEDs generated using the simplifications and the full dust treatment actually decreases gradually as the galaxy gets younger, since the dust properties adopted by following the assumptions are closer to their true values at earlier times (Fig. 12). The disparity introduced from assuming a dust-to-gas scaling relation (Fig. 11b) always dominates the disparity from assuming a constant chemical composition (Fig. 11a) and the disparity is always largest in the FIR.

The dust size distribution in irregular galaxies is likely to differ from that of the Milky Way (e.g. Galliano et al. 2005). This is highlighted by the fact that extinction curves have been observed in both the Small Magellanic Cloud (SMC) and Large Magellanic Cloud and have been found to differ from that of the Milky Way. The SMC extinction curve is of particular interest since it is an irregular dwarf galaxy with a substantially lower metallicity than the Milky Way and should represent a dust environment similar to our theoretical irregular model. The predicted extinction curve for the mass and composition of dust predicted by our irregular model has been compared to the observed SMC curve in order to constrain a dust grain size distribution. As Fig. 14 shows just by adopting the chemical composition predicted by the full CPM08 model even with the size distribution already calculated to match the properties of the Milky Way, a reasonable fit is obtained to the extinction curve, so that the different chemical composition alone can go some way in explaining the observed extinction curve. By fine-tuning the parameters governing the size distribution in equation (7), an improved fit can be obtained, as shown in the figure. The values of the best-fitting parameters are shown in Table 1.

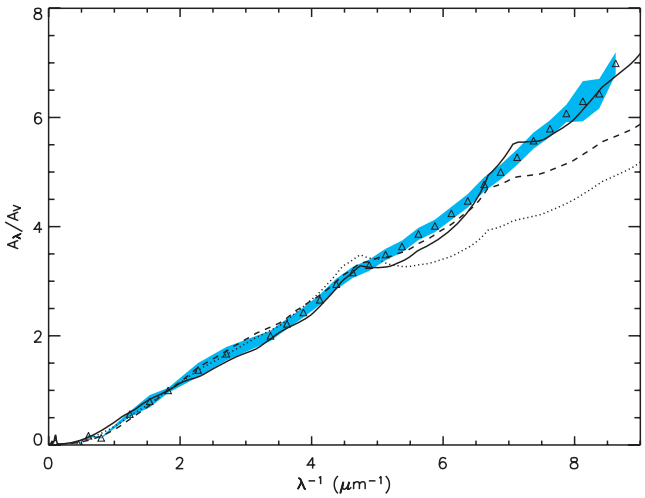

Figure 14. Best-fitting dust composition to SMC extinction curve. Solid line – full CPM08 model with optimized size distribution; dashed line – full CPM08 with S98 size distribution; dotted line – Milky Way chemical composition, S98 size distribution . The blue shaded area shows the associated uncertainty in the observed extinction curve.

Fig. 15 displays a comparison of the SEDs for the full model adopting the size distribution constrained using the SMC extinction curve to the SEDs for the full model using the standard Milky-Way-derived size distribution. It shows that the difference is small at all times, largely because the difference in the two size distributions is small.

Downloaded from https://academic.oup.com/mnras/article/394/4/2001/1203297 by guest on 20 August 2022

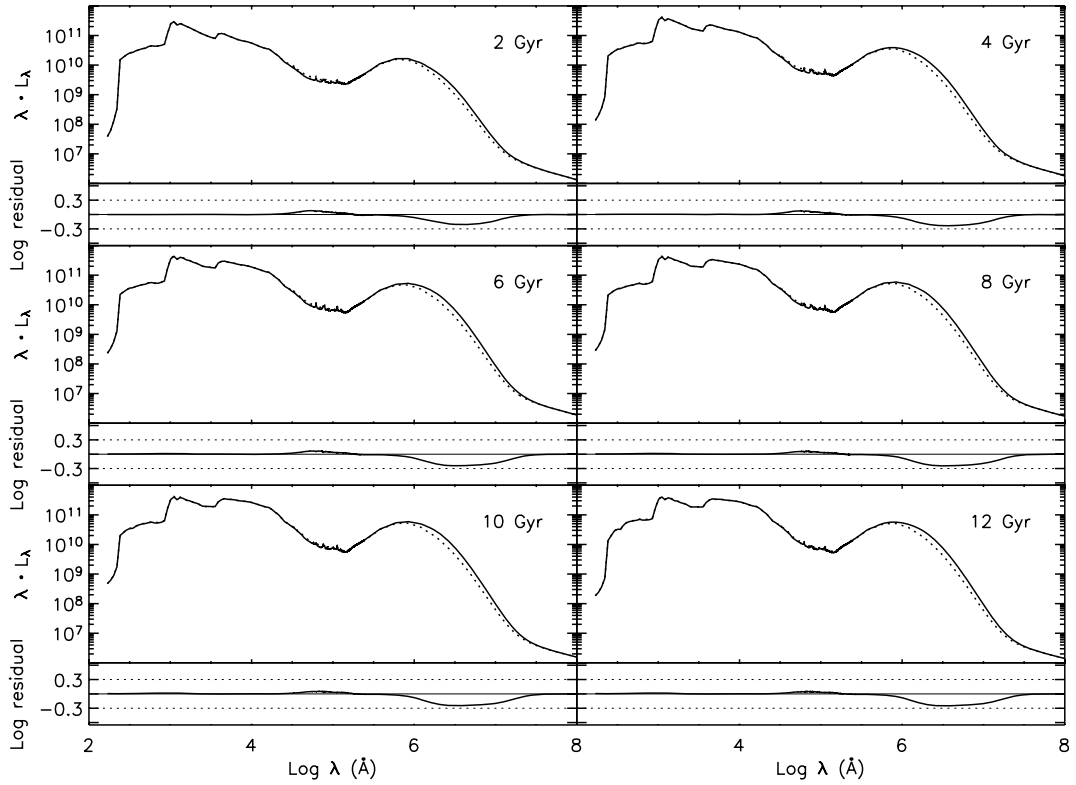

Figure 15. The effect of the SMC size distribution on the evolution of the SED of the irregular galaxy, solid line full CPM08 model with MW size distribution, dashed line – full CPM08 model with SMC size distribution.

4.3 Properties of elliptical galaxies

In our elliptical galaxy formation scenario, there are two distinct stages. An initial rapid collapse of a sphere of primordial gas leading to intense star formation and a second quiescent stage where the star formation has stopped as almost all of the gas is blown away by galactic winds. These two stages will be discussed separately. Unless stated, all results shown are for the elliptical model with a final stellar mass of 10^{11} $M_{\odot}$.

4.3.1 Starbursting phase – high redshift

The evolution of the SED of our elliptical model during the starbursting phase is shown in Fig. 16. Initially, all the stars will be located within their birth clouds (MCs); however since the dust mass is initially negligible the SED at these very early times will have the form of just the bare stellar component. The MCs will soon become rapidly enriched with dust due to dust production in Type II SNe, and as a result the reprocessing will rise quickly, almost to 100 per cent after 0.005 Gyr (Fig. 7). As the ages of the galaxies increase more stars will have time to escape from their MCs and as a result will be radiating in the more diffuse cirrus; hence there is a gradual decrease in the reprocessing observed in the figure. The small amount of PAH emission seen in the SEDs of Fig. 16 is as a result of the large proportion of dust emission coming from the MCs. Due to the suppression of the abundance of PAHs in these environments, they will consequentially produce little PAH emission. After the onset of the galactic winds at 0.7 Gyr, the majority of the dust is blown out of the galaxy so that the amount of reprocessing drops, at the same time the star formation is stopped and the galaxy enters the passively evolving stage.

Fig. 17 shows the effect that the two simplifications will have on the SEDs. Of the two, adopting the assumption that the dust-to-gas ratio will scale with the metallicity will have the biggest effect. This is because as Fig. 18b shows that although such a relationship does hold for these young galaxies initially (ages < 0.3 Gyr), the dust-to-gas value calculated by the model soon diverges from the expected value based on the metallicity, and as a result using this simplifications leads to large disparities in the SEDs.

Assuming a Milky Way chemical composition for the dust, however, has little effect on the SEDs at early times. This is because as Fig. 18a shows the chemical composition, at least initially, is remarkably similar to the value of 0.19 calculated for the solar neighbourhood. As the burst progresses, the C/Si begins to drop leading to small differences between the SEDs of the full CPM08 model and the simple dust model (see Fig. 17a).

Although the model calculates that the chemical composition of the total dust component is likely to be quite similar to that of the solar neighbourhood throughout the burst, it does not necessarily follow that the individual grains will be of the same composition and have the same size distributions as that observed locally. In the local universe, much of the dust is thought to be produced in the stellar winds of low- and intermediate-mass stars. However, in young galaxies at high redshift with ages less than 1 Gyr, such stars would not have had sufficient time to evolve to this stage, instead the dust will be predominantly produced in SNe (for detailed information of the relative production rates of the various mechanisms, see figs 2 and 6 in CPM08). Hence, the dust properties in these young galaxies are thought to be very different from that observed in the local universe in the Milky Way and in the SMC.

One possible tool for the study of dust in the high-redshift universe is QSOs. According to recent models of QSO–galaxy

Downloaded from https://academic.oup.com/mnras/article/394/4/2001/1203297 by guest on 20 August 2022

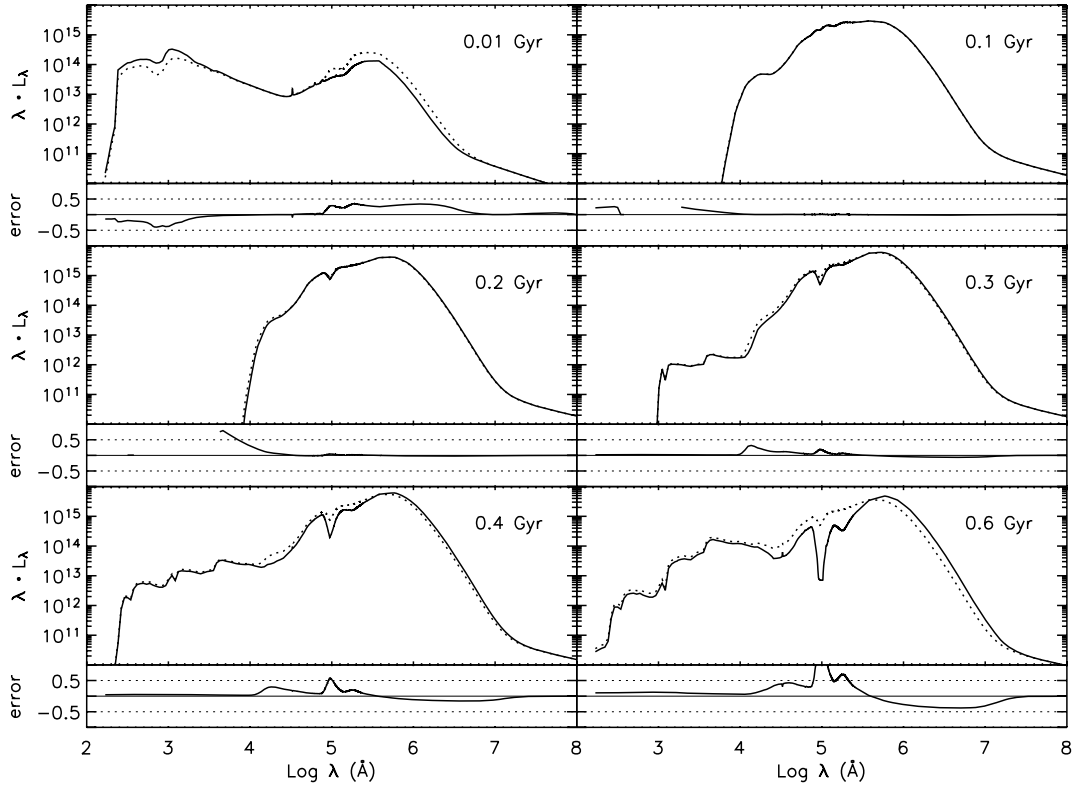

Figure 16. The high-redshift evolution of the SED of the elliptical galaxy, panels are the same as for Fig. 6.

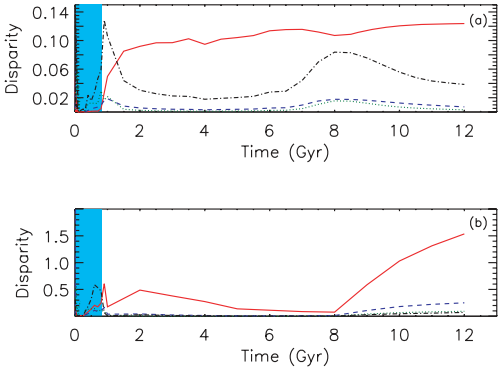

Figure 17. The residuals between the SEDs generated by the full elliptical CPM08 model and SEDs generated by using the simplifications that (a) the chemical composition remains equal to the Milky Way values at all times, (b) the dust-to-gas ratio scales with the metallicity. Lines are the same as in Fig. 9. The blue shaded area represents the age before the galactic wind starts in the elliptical model during which it is undergoing a period of extreme star formation.

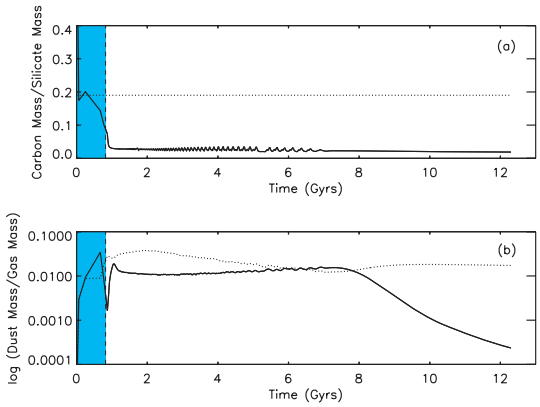

Figure 18. Elliptical galaxy. (a) Comparison between the value of the C/Si calculated by the full CPM08 ratio (solid line) with the constant value assumed if the chemical abundance remains identical to the present value for the solar neighbourhood (dotted line). (b) Comparison of the dust-to-gas ratio value calculated by the full CPM08 model (solid line) with the expected value if a dependence on the metallicity is assumed (dotted line). The blue shaded area represents the age before the galactic wind starts in the elliptical model during which it is undergoing a period of extreme star formation.

coevolution (e.g. Granato et al. 2004; Di Matteo, Springel & Hernquist 2005) during the early stages of galaxy and black hole growth, the AGN is embedded in gas and dust and is therefore difficult to identify as a QSO; however after the onset of galactic winds because large quantities of dust and gas will be swept away the QSO can be observed. The properties of observed QSOs should therefore be predicted by our elliptical model at times shortly after the onset of the galactic wind. Maiolino et al. (2006) showed that the chemical abundances observed in QSOs best match the chemical abundances calculated for our giant 10^{12} $M_{\odot}$ elliptical model at times later than 0.5 Gyr corresponding to the epoch just after the onset of the galactic winds supporting this theory. By studying the SEDs of QSOs, it has been possible to infer extinction curves for these objects, and by studying these observed curves it should be possible to constrain a size distribution for our young elliptical galaxies.

Maiolino et al. (2004) calculated an extinction curve for a high-redshift QSO, SDSS J1048+46, at a redshift of $z = 6.193$ and found that the extinction curve differs greatly from the extinction curves

Downloaded from https://academic.oup.com/mnras/article/394/4/2001/1203297 by guest on 20 August 2022

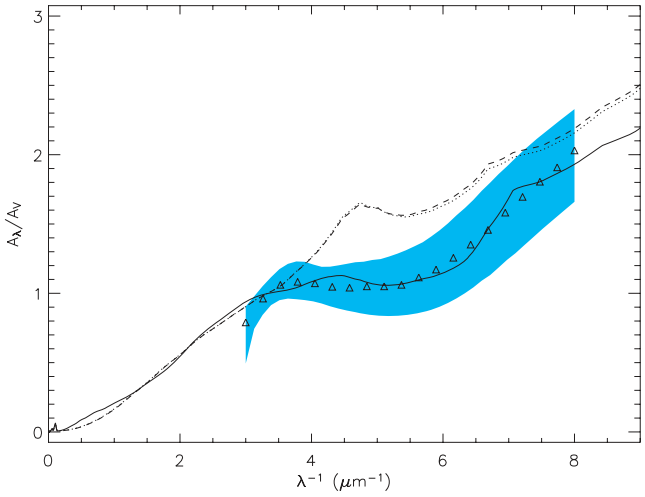

Figure 19. Best-fitting dust composition to the SDSS 1048 +46 quasar extinction curve. Solid line – full CPM08 model with optimized size distribution; dashed line – full CPM08 with S98 size distribution; dotted line – Milky Way chemical composition, S98 size distribution. The blue shaded area shows the associated uncertainty in the observed extinction curve.

observed at low redshift. The observed extinction curve has been compared to the extinction curve predicted by several models which have been written to predict the size distribution of dust from SNe, including Bianchi & Schneider (2007) and Nozawa et al. (2007). These size distributions have been found to be consistent with the observed QSO extinction curve, leading to the conclusion that the dust observed in the extremely high-redshift objects could indeed be dominated by SNe dust. The processes involved in the formation of dust in SNe are complicated and far from being completely understood. Indeed, the size distributions predicted by Nozawa et al. (2007) and Bianchi & Schneider (2007) differ substantially from each other. In addition, both papers only consider the production and destruction of dust in SNe, neither follow the accretion and destruction of the SNe remnants in the ISM as well as that by the galactic winds.

In this paper, starting from the dust masses calculated by the CPM08 $10^{12}\,M_\odot$ elliptical model, at a galactic age of 0.5 Gyr, the parameters in equation (7) which correspond to the best fit to the Maiolino et al. (2004) extinction curve at $Z \sim 6$ have been calculated. The resultant extinction curve is shown in Fig. 19. The best-fitting parameters are shown in Table 1.

Fig. 20 shows the effect that adopting this size distribution will have on the SEDs of elliptical galaxies during their starburst phase. The SEDs generated vary substantially from those generated using the Milky Way size distribution particularly in the NIR and MIR.

4.3.2 SCUBA galaxies

The theoretical SEDs for the $10^{11}\,M_\odot$ young elliptical galaxies are compared to SCUBA galaxies at high redshifts. These galaxies have been found to be dust-enshrouded sources with very high SFRs. It is believed that these SCUBA galaxies could represent the birth of giant elliptical galaxies (Lilly et al. 1999; Eales et al. 2000) and should therefore correspond to the starbursting phase of our elliptical models. The data used are from the SCUBA Half Degree Extragalactic Survey (SHADES) survey of the Suburu/*XMM–Newton* field Deep Field (SXDF) (Clements et al. 2008). This survey is ideal for the purposes of this paper since it has a good photometric coverage with observations from the optical SXDF (*B*, *V*, *R*, *i*′ and *z*′), *Spitzer* (Infrared Array Camera (IRAC) 3.6, 4.5, 5.8, 9 μm and Multi-band Imaging Photometer for Spitzer (MIPS) 24, 70 and 160 μm) and SCUBA. Only the galaxies with the highest redshift from the sample were used, namely galaxies which were found by Clements et al.

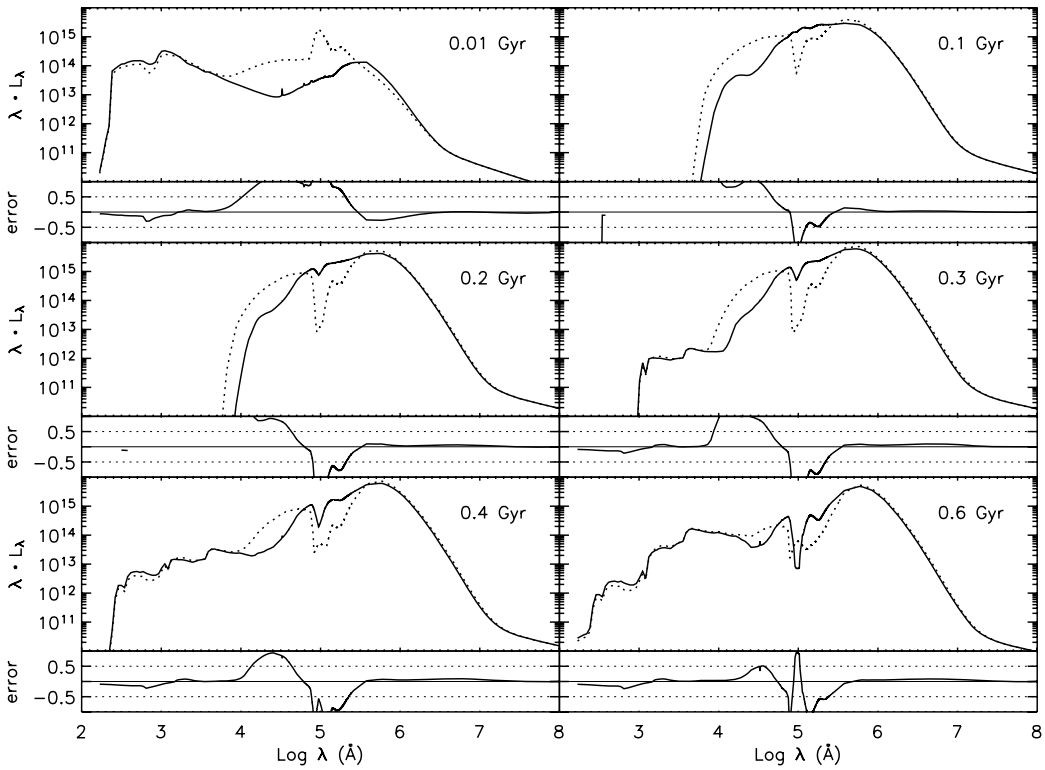

Figure 20. The effect of the quasar size distribution on evolution of the SED of the young elliptical galaxy: solid line – full CPM08 model with MW size distribution and dashed line – full CPM08 model with the dust consistent with the $z \sim 6$ QSO.

© 2009 The Authors. Journal compilation © 2009 RAS, MNRAS **394,** 2001–2021

Downloaded from https://academic.oup.com/mnras/article/394/4/2001/1203297 by guest on 20 August 2022

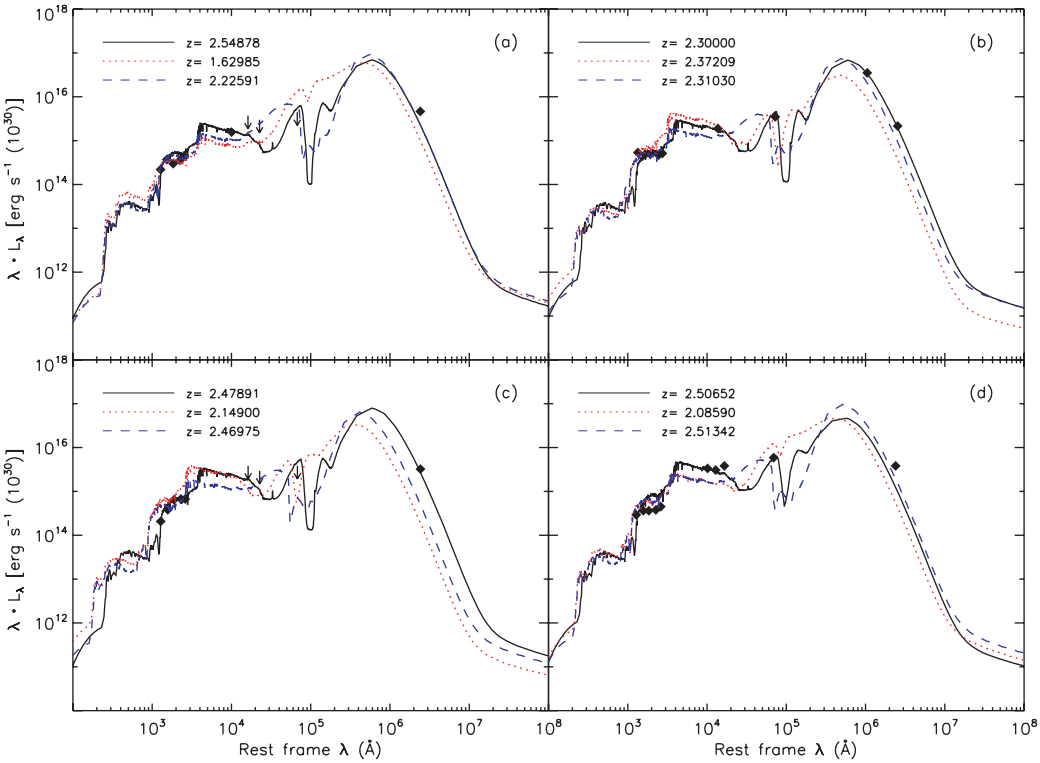

Figure 21. Comparison of $10^{12}\,M_{\odot}$ theoretical elliptical model with the SED of SCUBA galaxies. (a) SHADES-SXDF 10, (b) SHADES-SXDF 11, (c) SHADES-SXDF 12, (d) SHADES-SXDF 7. Solid line – full CPM08 model. Dotted line – simple dust model. Dashed line – full CPM08 model with dust consistent with the $z \sim 6$ QSO. The rest-frame wavelength is correct for the redshift calculated for the full CPM08 model. The abscissa values for the curves for the simple dust model and the full CPM08 model with dust consistent with the $z \sim 6$ QSO were appropriately rescaled. The redshift values calculated by Clements et al. (2008) are $z = 2.08$ for SHADES-SXDF 10, $z = 2.30$ for SHADES-SXDF 11, $z = 3.07$ for SHADES-SXDF 12 and $z = 2.31$ for SHADES-SXDF 7.

(2008) to have a photometric redshift greater than 2. In total, these galaxies numbered 13.

Fig. 21 shows that for four of the observed galaxies in the SHADES data set our model was able to match the general shape of the SED and the observed amount of reprocessing. The average age of the best-fitting full CPM08 models for the four galaxies shown is 0.55 Gyr. At such an age, the theoretical model will still have ongoing star formation. Because only one star formation history has been followed and no parameters varied, perfect matches could not be expected to all observed galaxies. However, as shown, even with this one simple star formation history, the observed SEDs of four out of the 13 galaxies investigated in this work could be reasonably reproduced. This suggests that the rationale of treating these galaxies as obscured starbursts with a dust mass calculated by the CPM08 model is consistent with the observations. Also shown in the figure are the spectra for the simple dust model and for the full dust model with the dust composition calculated in order to fit the QSO SDSS J1048+46. Although the SEDs generated using the full model with the size distribution consistent with the $z \sim 6$ QSO diverge from that of the full CPM08 model significantly, the theoretical SEDs are still largely consistent with the data. The SEDs generated by the simple dust model on the other hand lead to slightly worse fits, although a much more thorough analysis is needed to come to a more definite conclusion.

4.3.3 Giant post-starburst galaxies at high redshift

The theoretical SEDs calculated for young elliptical galaxies are compared to massive galaxies which have been observed to be already highly evolved at high redshifts (Wiklind et al. 2008). Since these galaxies are likely to be massive, the giant $10^{12}\,M_{\odot}$ elliptical galaxy will be used in the fits. The galaxies in the data set have been selected by Wiklind et al. (2008), so that they are dominated by a stellar population older than ∼100 Myr and situated at $z \geq 5$. They should therefore correspond to a later stage in the evolution of our elliptical galaxy model, the post-starburst stage of our giant elliptical model. Data points are available in the optical (Advanced Camera for Surveys (ACS) – B, V, i, z) NIR (the Infrared Spectrometer and Array Camera (ISSAC) and the VLT – J, H, K_s) and MIR (deep imaging with the Spitzer Space Telescope with IRAC-3.4, 4.5, 5.7, 8.9 μm and MIPS – 24 μm). For the chi-squared fitting, the point at 24 μm was not included since emission in this region could be dominated by an AGN.

Many of the observed galaxies could be well matched by our theoretical model, and Fig. 22 shows good fits to four of the galaxies in the sample. The fits for the full CPM08, the simple dust model and the full dust model with the dust composition calculated in order to fit the QSO SDSS J1048+46 are all good. The theoretical SEDs diverge from each other mostly in the rest-frame FIR, and since no observations exist for this part of the spectrum the difference in fits in the SEDs is slight. The average age of the best-fitting full CPM08 models for the four galaxies shown is 0.61 Gyr. At such an age, our giant elliptical model corresponds to a post-starbursting system with no current star formation. It should be noted that because only one star formation history was followed in this work, our calculated value for the stellar ages of the galaxies should be taken as an indication of one possible formation scenario not as an actual value.

Downloaded from https://academic.oup.com/mnras/article/394/4/2001/1203297 by guest on 20 August 2022

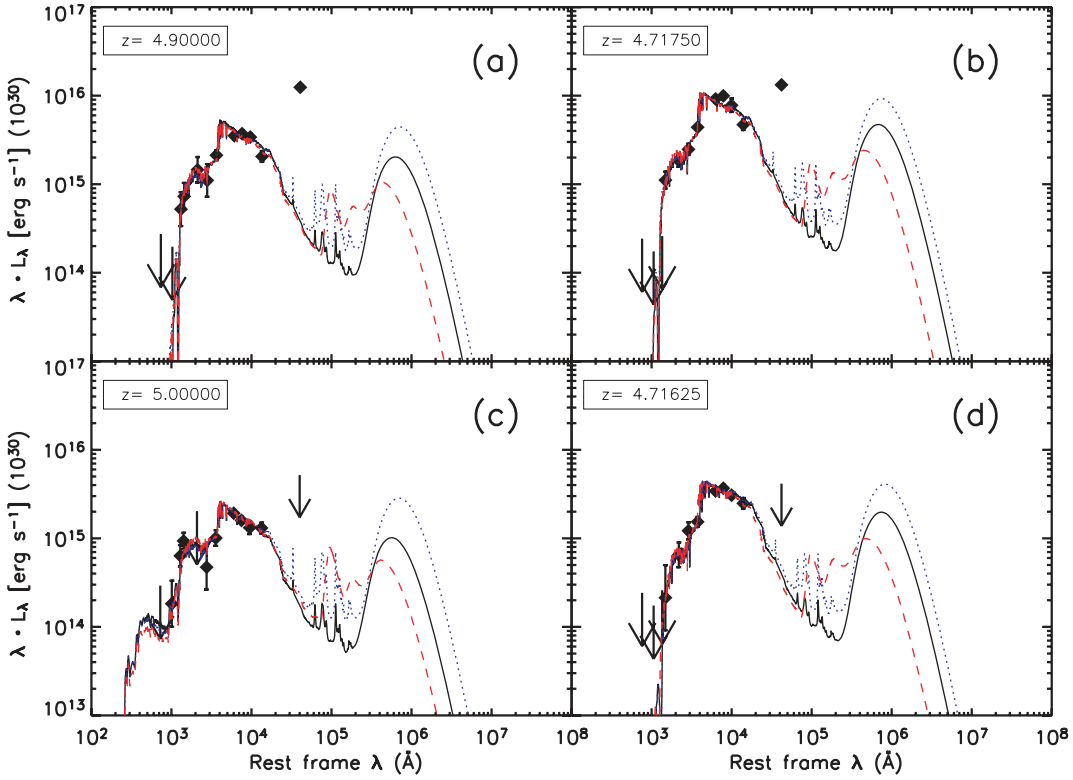

Figure 22. Comparison of the 10^{12} $M_{\odot}$ theoretical elliptical model with the SED of balmer break galaxies. (a) BBG 2910, (b) BBG 3348, (c) BBG 3361, (d) BBG 4071. Black solid line – full CPM08 model. Blue dotted line – simple dust model. Red dashed line – full CPM08 model with dust consistent with the $z \sim 6$ QSO. The rest-frame wavelength is correct for the redshift calculated for the full CPM08 model, the value given in the top-left corner of the panel. In all cases, the redshift values were the same for the two other models; except for BBG 4071, where a redshift of 4.348 75 was calculated for the simple dust model, the abscissa values for the curve were appropriately rescaled. The redshift values calculated by Wiklind et al. (2008) are $z = 4.9$ for BBG 2910, $z = 5.1$ for BBG 3348, $z = 5.0$ for BBG 3361 and $z = 5.0$ for BBG 4071.

For several of the galaxies in the sample, intriguingly the observed MIPS flux at 24 μm far exceeds the flux predicted by our model, e.g. BBG 3348. This galaxy has been observed in the X-ray with a luminosity of 3×10^{43} erg s^{-1}, and it is therefore plausible that the observed MIPS flux could have a contribution from an obscured AGN. Such a source could explain the higher flux observed in this band but would have a minimal impact on the part of the SED covered by the ACS/ISAAC/IRAC bands (see e.g. Mobasher et al. 2005) and would therefore not affect the presented SED fit in this region.

Fig. 23, however, shows an alternative formation scenario for this galaxy, in which the predicted SED of the 10^{11} $M_{\odot}$ model is normalized and compared to the observed SED. The best-fitting model has been found to have a stellar age of 0.6 Gyr, the same age as that calculated for the 10^{12} $M_{\odot}$ model. As can be seen from the fit, the MIPS 24 μm flux is predicted by the model without the need of an obscured AGN. In this 10^{11} $M_{\odot}$ model, star formation is still ongoing at such an age. Due to the nature of the dust model used, this young star formation will be entirely obscured within dense MCs, so will only contribute to the flux in the rest-frame MIR and FIR. The older stars that have been able to escape the MCs, however, will be only slightly absorbed due to the less dense cirrus producing a similar SED in the optical and NIR as the 10^{12} $M_{\odot}$ model described above.

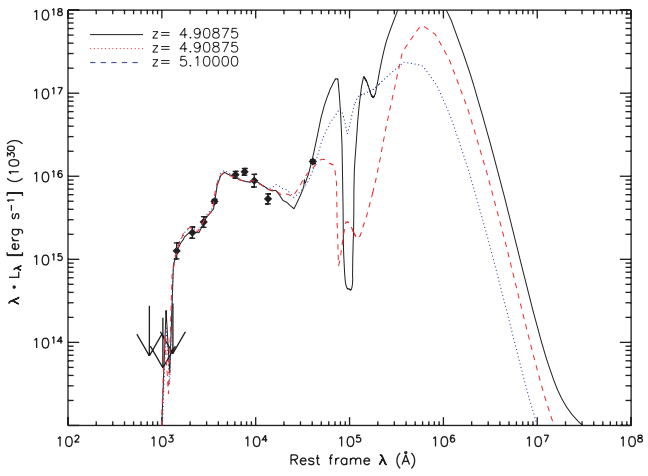

Figure 23. Comparison of the 10^{11} $M_{\odot}$ theoretical model with galaxy BBG 3348 from the Wiklund sample. Dotted line – simple dust model. Dashed line – full CPM08 model with dust consistent with the $z \sim 6$ QSO. The rest-frame wavelength is correct for the redshift calculated for the full CPM08 model. The abscissa values for the curves for the simple dust model and the full CPM08 model with dust consistent with the $z \sim 6$ QSO were appropriately rescaled. Wiklind et al. (2008) calculated a redshift value of $z = 5.0$.

Downloaded from https://academic.oup.com/mnras/article/394/4/2001/1203297 by guest on 20 August 2022

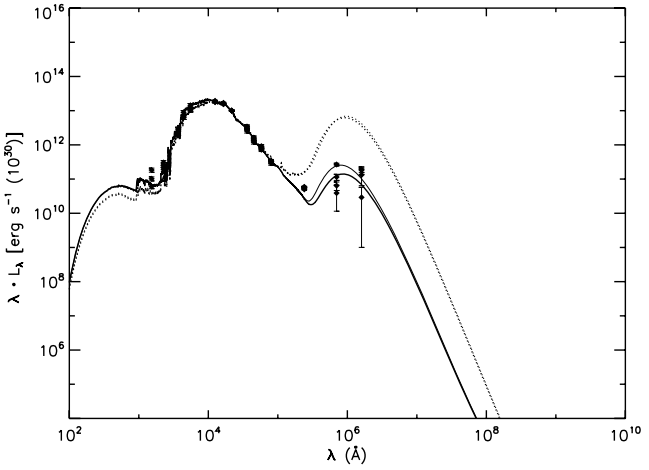

Figure 24. Comparison of theoretical elliptical model at 12 Gyr with an average SED taken from four elliptical galaxies of the SINGS sample. Solid line – full CPM08 model and dotted line – simple dust model. The thick line is for a scalelength of dust twice as large as that of the stellar component, while the thin line is for equal scalelengths.

Both scenarios described, obscured starburst or a passive galaxy with an AGN are equally consistent with the data. Longer wavelength observations would be required to discriminate between them.

4.3.4 Quiescent stage – low redshift

Fig. 24 shows the result for the theoretical SED of the elliptical model generated at 12 Gyr compared to the SEDs of the four 'passive' local elliptical galaxies from the SINGS sample. The SED generated by the model with the full dust evolution matches the observations well. Elliptical galaxies display fairly homogeneous optical colours, a trend reflected in the observed galaxies in Fig. 24, which have almost identical SEDs from the optical to the NIR. The SED in this region is reproduced well by our full theoretical model and also the simple dust model. The four galaxies though show larger scatter in the FIR and UV.

Although there is much scatter in the observed FIR bump, probably due to a differing dust content, the full CPM08 model predicts FIR emission which agrees well with the average of the observed points. It can therefore be thought of as having a dust content consistent with this sample. However, when the simple dust model using the two simple dust assumptions is used, SEDs are generated which significantly overestimate the amount of FIR observed, presumably because of the larger dust content present, due to the assumption that the dust-to-gas ratio scales with the metallicity (see Fig. 18b). In this work, an assumption has been introduced that the dust component is more extended than that of the stellar component with a scalelength twice as large (see Section 3.3.4). To check the robustness of our results on this assumption, the SED of the elliptical model at 12 Gyr with a scalelength of the dust equal to that of the stellar component was calculated. This is also shown in Fig. 24, and it can be seen that although this assumption does have a notable effect on the SED, the fit for the full CPM08 model is still consistent with the observations while the simple dust model still overpredicts the emission in the FIR.

Out of the four 'passive' elliptical galaxies in the sample all four have observations in the near-UV and three have observed points in the far-UV. Although the galaxies do show a small amount of scatter in this region, the theoretical model is able to reproduce an UV upturn which is consistent with the average points. The UV scatter too could be partially explained by differing amounts of extinction due to different dust contents. Indeed, the simple dust model seems to underpredict the luminosity in the FUV, presumably because of the greater dust content present. However, it has also been claimed by several authors (e.g. Kaviraj et al. 2007) that the range of UV colours observed in different early-type galaxies could be due to a small amount of recent star formation (1–3 per cent) in a large proportion of galaxies. This, however, is beyond the scope of this paper.

The theoretical evolution of the SED of the elliptical galaxy is shown in Fig. 25. Young stars are the main contributors to the UV so since there is no star formation the elliptical galaxies are weak in the UV. The amount of reprocessing in the galaxy (Fig. 7) is always small, at all times less than 5 per cent, and follows the mass of dust present in the galaxy (Fig. 3b), so it peaks at approximately 8 Gyr and then declines due to destruction from the X-rays emitted by the hot gas.

Fig. 17 shows that of the two simplifications the largest effect on the SEDs comes from assuming the dependence of the dust-to-gas ratio on the metallicity which will lead to large disparities in the SED. This is because this assumption leads to large differences in the dust-to-gas ratio with the results obtained from the full CPM08 model (see Fig. 18b). As Fig. 17 shows, the disparity will be largest in the FIR.

5 IMPLICATIONS OF THIS WORK

In this work, only one likely chemical and dust evolution model, with one star formation history, has been followed for each morphological type of galaxy based on average properties of the galaxy type as a whole. It is therefore not possible to conclusively prove the accuracy of the models, since it is unlikely that they will exactly match the SED of any one specific galaxy. However, since the chemical evolution models are designed to match average properties, the generated SEDs would be expected to match the general appearance of many galaxies of the specific type, and this is indeed what has been found. In this paper, plots have been presented which show acceptable fits to local spirals, irregulars and ellipticals simultaneously in their starbursting, post-starbursting and passive phase. It should also be noted that although both models contain many parameters, very little fine-tuning has been performed to fit observations. Instead, the parameters have been set either to physically reasonable values based on observations or to values which, when used previously, have been found to give good fits to observations. As a result, the fits are remarkably good and, although far from conclusive, seem to validate both the chemical evolution model used (the CPM08 model) and the stellar population model adopted (GRASIL). Only two parameters were tuned in this work to match the observations. For the irregular galaxies, in order to fit the MIR part of the SEDs of local dwarf irregulars the optical depth of the molecular clouds (MCs) in which the stars are born needed to be reduced to a lower optical depth than the MCs in normal star-forming galaxies. It is not possible to say whether the improved fit requires a lower MC mass or a larger MC radius because the optical depth is dependent on both the mass and the radius and is given by $M_{\rm mc}/R^2_{\rm mc}$. For the elliptical galaxies, to match the large amount of reprocessing observed in the SEDs of the SCUBA galaxies in the SHADES data set, the time spent initially by the young stars in the dense MCs was increased to a larger value than that found for local normal star-forming galaxies.

Downloaded from https://academic.oup.com/mnras/article/394/4/2001/1203297 by guest on 20 August 2022

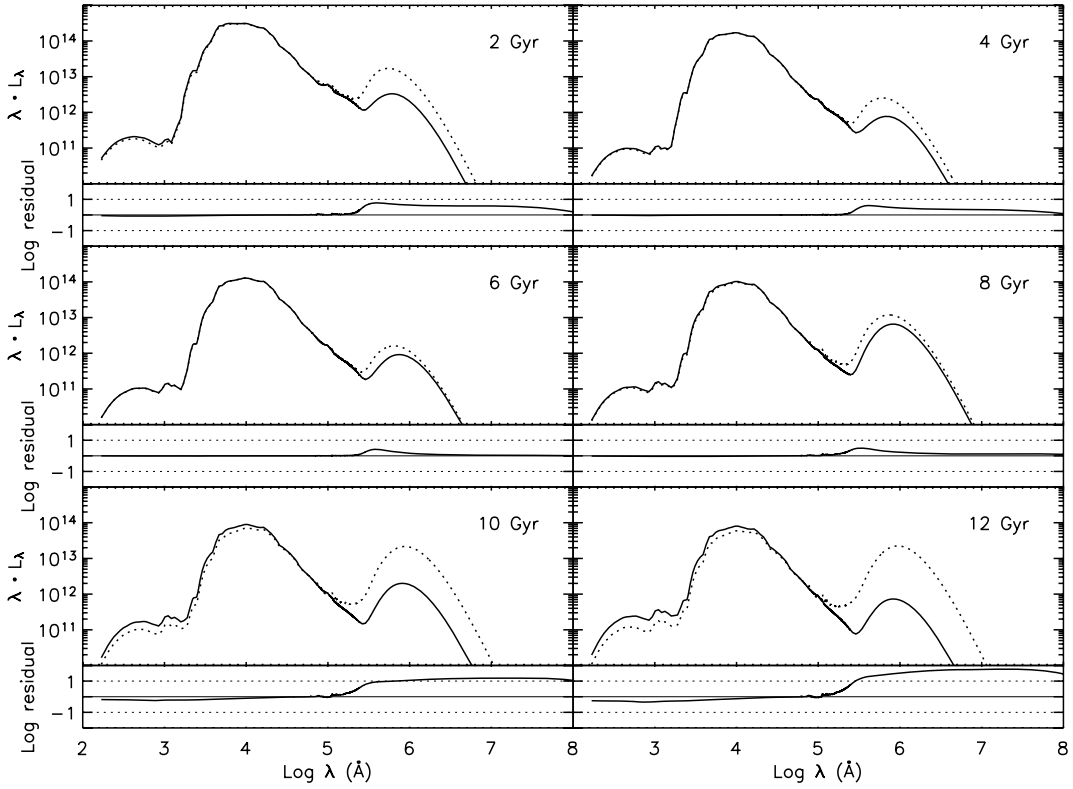

Figure 25. The evolution of the SED of the elliptical galaxy, panels are the same as for Fig. 6.

In the CPM08 paper, it was found that the dust depletion pattern is determined by the balance between destruction and accretion, and since neither process can be constrained accurately from the solar neighbourhood, nothing definite can be learned about the rate of either. However, in both the elliptical and irregular galaxies the accretion rates should be negligible, hence by studying such environments it should, in theory, be possible to derive constraints for the destruction rates of the different elements. The reasonable fits to local galaxies support the values chosen.

The use of theoretical template SEDs in comparisons with photometry has proved to be a useful tool in order to gain insights into high-redshift galaxies, in particular for determining a photometric redshift (e.g. Rowan-Robinson et al. 2008). Among the templates commonly used are those of well-studied starburst galaxies in the local universe, such as ARP 220 and M82. However there is evidence that starburst galaxies at high redshift display different characteristics to their low-redshift counterparts, for example showing higher specific star formation rates (star formation rate/stellar mass) (Bauer et al. 2005) and higher dust obscuration rates (Hammer et al. 2005). It is therefore important to develop a set of multiwavelength templates specific to the type of galaxy expected at high redshift, particularly with the approaching launch of the European Space Agency's Herschel Space Observatory (Pilbratt 2005), which will increase the wavelength coverage for these objects. Our models deal with both the chemical and dust evolution in these early galaxies in a self-consistent way, and in this paper the SEDs generated have been shown to match high-redshift galaxies simultaneously in both the starbursting and post-starbursting stage. They should therefore provide ideal templates for the analysis of these high-redshift galaxies. Further work will be carried out to generate and test a range of high-redshift templates.

Also investigated in this work are the potential errors you could expect by introducing two common simplifications into the modelling of galaxies: that the dust-to-gas mass ratio is proportional to the metallicity, and that the dust composition in all galaxies is equal to that derived for the Milky Way. These *errors* are given as the difference between our fiducial models with the detailed dust treatment and the models using the two simplifications. They will only be correct for the models presented here and not for any real galaxy in particular. However, the chemical evolution models have been thoroughly tested against observations in previous works, and in this paper the SEDs have been shown to be broadly consistent with the SEDs of the modelled morphological type. Therefore, the disparities presented in this work can be viewed as an example of the magnitude of errors that could be expected if the simplifications are adopted in spiral, irregular and elliptical galaxies. In particular, it has been shown that for spiral galaxies the errors that could be expected are small and decrease with the age of the galaxy; this is unsurprising since these simplifications have been developed based on the Milky Way in the case of the chemical composition and observations on local star-forming galaxies in the case of the dust-to-gas ratio. For irregular and elliptical galaxies, however, it has been shown that potentially the disparities introduced by adopting the two simplifications could be much larger. Of the two simplifications, it has been shown that in both galactic types the simplification likely to lead to the largest disparities is assuming the dependency on the metallicity of the dust-to-gas ratio, and that the largest disparities would be expected in the IR part of the spectrum.

The main limitation of this work is that only the total mass in each of the main dust species is followed. The model does not calculate in what proportions they combine to make up dust grains, and what the size distribution of these dust species could be. As a result, a

Downloaded from https://academic.oup.com/mnras/article/394/4/2001/1203297 by guest on 20 August 2022

major assumption had to be introduced for the composition of the dust grains: that the size distribution does not evolve and all times will be identical to that calculated to match properties of the Milky Way (the S98 size distribution). This assumption was relaxed in irregular galaxies where a dust composition consistent with the SMC extinction curve was calculated and in young elliptical galaxies where a dust composition consistent with the extinction curve of a high-redshift QSO was found. It was shown that adopting the dust composition based on the SMC had only a small effect on the SEDs. The effect of adopting the dust composition consistent with the QSO in young elliptical galaxies had a large effect particularly in the NIR and MIR. With the current observational data, it was not possible to put strong constraints on which size distribution is the more realistic, but the huge difference in the SEDs generated using the two different distributions highlights how important using the correct size distribution could be and how it could have large consequences for surveys or any observations taken shortwards of the peak of the dust emission; precisely the wavelength range which the Herschel Space Observatory is set to operate in.

6 SUMMARY AND CONCLUSIONS

Starting from the models proposed in the CPM08 paper, the chemical and dust evolution models have been combined with the GRASIL spectrophotometric population synthesis code in order to generate SEDs for the solar neighbourhood and irregular and elliptical galaxies from the birth of the galaxy to an age of 13 Gyr.

The SEDs have been compared where possible to observed SEDs. A good fit has been obtained for the spiral model when compared to local spiral galaxies, the elliptical model has simultaneously fitted observations of high-redshift starbursting (SCUBA) galaxies, high-redshift post-starburst galaxies and local galaxies, while the irregular galaxy model has been shown to adequately match the SEDs of local irregular galaxies of Magellanic type. The results are particularly remarkable since very few of the GRASIL parameters were fine-tuned in order to obtain these results, instead they were merely set to a combination of observationally motivated values or to values which have been found to give good fits to observations in previous works. The good fits give further indications that the galaxy formation scenarios chosen for each morphological type in order to fit the chemical properties of these galaxies are indeed valid. In addition, the good fits particularly to the local elliptical and irregular galaxies suggest that the dust treatment adopted in the CPM08 paper is reliable and in particular supports the destruction and accretion rates chosen. From these fits to observations, it has been shown that the optical depth in MCs in irregular galaxies is likely to be lower than that of normal star-forming galaxies. It has also been found that in order to match the observations of SCUBA galaxies the stars in the young extreme starbursting galaxies initially spend a large period of time in dense MCs before escaping.

It has been shown that SEDs generated using either the assumption that the dust grain distribution in all environments is equal to that of the Milky Way or the assumption that the dust-to-gas mass ratio scales with the metallicity differ from those calculated using a full dust evolution model. Of these assumptions, it has been found that assuming a dust-to-gas ratio will introduce the largest disparities while the disparities introduced from an assumed chemical composition are small, only having a potentially large effect in the MIR, due to a change in the abundance of PAH molecules. For spiral galaxies, the disparities incurred by adopting the assumptions are small and will decrease with age and therefore increase with redshift, to a large part due to the normalization of the assumptions in this model to the results calculated for the spiral galaxy at 13 Gyr. The disparities introduced by adopting the assumptions are more significant in the galaxies of the two other morphologies at all ages, particularly in elliptical galaxies and therefore dust assumptions tuned to match those of the Milky Way should be used with caution in these galaxies.

It has also been shown that while using a Milky Way size distribution to model irregular galaxies should be a reasonable simplification, for elliptical galaxies at high redshift such a simplification could potentially lead to large errors.

The reasonable fit of the young elliptical galaxy to SCUBA galaxies at a redshift of $\sim$2.2 and to a massive post-starburst elliptical at a redshift of $\sim$5 suggests that the starbursting scenario adopted in this work is a reasonable one and that models generated by these models could act as useful templates to fit to high-redshift galaxies.

This study can be thought of as a first step towards a more careful comparison between galaxy formation scenarios and observed data, particularly in the spectral regions affected by dust emission. The robustness of such a comparison has clearly been shown to be affected by a proper treatment of dust evolution and reprocessing in a wavelength-dependent way. A more rigorous dust treatment which can be applied to galaxy formation models will be the subject of future papers.

ACKNOWLEDGMENTS

We are indebted to an anonymous referee, whose insightful comments have improved the quality of this paper. This work was supported through a Marie Curie studentship for the 6th Framework Research and Training network MAGPOP, contract number MRTN-CT-2004-503929. FC, LS, AP, GLG, FM and RM acknowledge partial support by ASI through contract ASI-INAF I/016/07/0.

REFERENCES

Bauer A. E., Drory N., Hill G. J., Feulner G., 2005, ApJ, 621, L89
Baugh C. M., Lacey C. G., Frenk C. S., Granato G. L., Silva L., Bressan A., Benson A. J., Cole S., 2005, MNRAS, 356, 1191
Beelen A., Cox P., Benford D. J., Dowell C. D., Kovacs A., Bertoldi F., Omont A., Carilli C. L., 2006, ApJ, 642, 694
Bell E. et al., 2005, ApJ, 625, 23
Bertoldi F., Carilli C. L., Cox P., Fan X., Strauss M. A., Beelen A., Omont A., Zylka R., 2003, A&A, 406, L55
Bianchi S., 2007, A&A, 471, 765
Bianchi S., Schneider R., 2007, MNRAS, 378, 973
Bianchi S., Davies J. I., Alton P. B., 2000, A&A, 359, 65
Bower R. G., Benson A. J., Malbon R., Helly J. C., Frenk C. S., Baugh C. M., Cole S., Lacey C. G., 2006, MNRAS, 370, 645
Bradamante F., Matteucci F., D'Ercole A., 1998, A&A, 337, 338
Bressan A., Chiosi C., Fagotto F., 1994, ApJS, 94, 63
Bressan A., Granato G. L., Silva L., 1998, A&A, 332, 135
Brinchmann J., Ellis R. S., 2000, ApJ, 536, L77
Calura F., Pipino A., Matteucci F., 2008, A&A, 479, 669 (CPM08)
Chiappini C., Matteucci F., Gratton R., 1997, ApJ, 477, 765
Chiappini C., Matteucci F., Romano D., 2001, ApJ, 554, 1044
Clayton G. C., Green J., Wolff M. J., Zellner, Nicolle E. B., Code A. D., Davidsen A. F., WUPPE Science Team, HUT Science Team, 1996, ApJ, 460, 313
Clements D. L. et al., 2008, MNRAS, 387, 247
Cowie L. L., Songaila A., Hu E. M., Cohen J. G., 1996, AJ, 112, 839
Dale D. A., Helou G., 2002, ApJ, 576, 159
Dale D. A., Helou G., Contursi A., Silbermann N. A., Kolhatkar S., 2001, ApJ, 549, 215
Dale D. A. et al., 2007, ApJ, 655, 863

Downloaded from https://academic.oup.com/mnras/article/394/4/2001/1203297 by guest on 20 August 2022

de Vaucouleurs G., de Vaucouleurs A., Corwin H. G. Jr, Buta R. J., Paturel G., Fouque P., 1991, Third Reference Catalogue of Bright Galaxies, Vol 1-3. Springer-Verlag, Berlin
Desert F.-X., Boulanger F., Puget J. L., 1990, A&A, 237, 215
Di Matteo T., Springel V., Hernquist L., 2005, Nat, 433, 604
Dopita M. A., 2005, in Popescu C. C., Tuffs R. J., eds, AIP Conf. Proc. 761, The Spectral Energy Distributions of Gas-Rich Galaxies: Confronting Models with Data. Am. Inst. Phys., New York, p. 203
Draine B. T., Lee H. M., 1984, ApJ, 285, 89
Draine B. T., Li A., 2001, ApJ, 551, 807
Draine B. T., Li A., 2007, ApJ, 657, 810
Draine B. T. et al., 2007, ApJ, 663, 866
Dunne L., Eales S., Ivison R., Morgan H., Edmunds M., 2003, Nat, 424, 285
Dunne L. et al., 2008, MNRAS, in press (arXiv0809.0887D)
Dwek E., 1998, ApJ, 501, 643
Dwek E., Galliano F., Jones A. P., 2007, ApJ, 662, 927
Eales S., Lilly S., Webb T., Dunne L., Gear W., Clements D., Yun M., 2000, AJ, 120, 2244
Efstathiou A., Rowan-Robinson M., 2003, MNRAS, 343, 322
Efstathiou A., Rowan-Robinson M., Siebenmorgan R., 2000, MNRAS, 313, 734
Engelbracht C. W., Gordon K. D., Rieke G. H., Werner M. W., Dale D. A., Latter W. B., 2005, ApJ, 628, L29
François P., Matteucci F., Cayrel R., Spite M., Spite F., Chiappini C., 2004, A&A, 421, 613
Galliano F., Madden S. C., Jones A. P., Wilson C. D., Bernard J.-P., Le Peintre F., 2003, A&A, 407, 159
Galliano F., Madden S. C., Jones A. P., Wilson C. D., Bernard J.-P., 2005, A&A, 434, 867
Galliano F., Dwek E., Chanial P., 2008, ApJ, 672, 214
Granato G. L., Lacey C. G., Silva L., Bressan A., Baugh C. M., Cole S., Frenk C. S., 2000, ApJ, 542, 710
Granato G. L., De Zotti G., Silva L., Bressan A., Danese L., 2004, ApJ, 600, 580
Guzman R., Gallego J., Koo D. C., Phillips A. C., Lowenthal J. D., Faber S. M., Illingworth G. D., Vogt N. P., 1997, ApJ, 489, 559
Hammer F., Flores H., Elbaz D., Zheng X. Z., Liang Y. C., Cesarsky C., 2005, A&A, 430, 115
Hauser M. G., Dwek E., 2001, ARA&A, 39, 249
Hopkins F. P., Hernquist L., 2008, ApJ, in press (astro-ph/0809.3789)
Hunt L., Bianchi S., Maiolino R., 2005, A&A, 434, 849
Itoh H., 1989, PASJ, 41, 853
Juneau S. et al., 2005, ApJ, 619, L135
Kaviraj S. et al., 2007, ApJS, 173, 619
Kennicutt R. C., 1989, ApJ, 344, 685
Kennicutt R. C., 1998, ApJ, 498, 541
Kimura H., Mann I., Jessberger E. K., 2003, ApJ, 582, 846
Kodama T. et al., 2004, MNRAS, 350, 1005
Krause O., Birkmann S. M., Rieke G. H., Lemke D., Klaas U., Hines D. C., Gordon K. D., 2004, Nat, 432, 596
Laor A., Draine B. T., 1993, ApJ, 402, 441
Lilly S. J., Eales S. A., Gear W. K. P., Hammer F., Le F'evre O., Crampton D., Bond J. R., Dunne L., 1999, ApJ, 518, 641
Lisenfeld U., Ferrara A., 1998, ApJ, 496, 145
McKee C. F., 1989, in Allamandola L. J., Tielens A. G. G. M., eds, Proc. IAU Symp. 135, Interstellar Dust. Kluwer, Dordrecht, p. 431
McLure R. J., Dunlop J. S., 2002, MNRAS, 331, 795
Madden S. C., 2005, in Popescu C. C., Tuffs R. J., eds, AIP Conf. Ser. Vol. 761, The Spectral Energy Distributions of Gas Rich Galaxies: Confronting Models with Data. Am. Inst. Phys., New York, p. 223
Madden S. C., Galliano F., Jones A. P., Sauvage M., 2006, A&A, 446, 877
Maiolino R., Schneider R., Oliva E., Bianchi S., Ferrara A., Mannucci F., Pedani M., Roca Sogorb M., 2004, Nat, 431, 553
Maiolino R. et al., 2006, Mem. Soc. Astron. Ital., 77, 643
Marconi A., Risaliti G., Gilli R., Hunt L. K., Maiolino R., Salvati M., 2004, MNRAS, 351, 169
Marigo P., Girardi L., Bressan A., Groenewegen M. A. T., Silva L., Granato G. L., 2008, A&A, 482, 883
Mathis J. S., Rumple W., Nordsieck K. H., 1977, ApJ, 217, 103
Matteucci F., 1994, A&A, 288, 57
Matteucci F., Tornambè A., 1987, A&A, 185, 51
Misiriotis A., Xilouris E. M., Papamastorakis J., Boumis P., Goudis C. D., 2006, A&A, 459, 113
Mobasher B. et al., 2005, ApJ, 635, 832
Morgan H. L., Edmunds M. G., 2003, MNRAS, 343, 427
Morgan H. L., Dunne L., Eales S. A., Ivison R. J., Edmunds M. G., 2003, ApJ, 597, L33
Nagashima M., Lacey C. G., Okamoto T., Baugh C. M., Frenk C. S., Cole S., 2005, MNRAS, 363L, 31
Noeske K. et al., 2007, ApJ, 660, L43
Nozawa T., Kozasa T., Habe A., Dwek E., Umeda H., Tominaga N., Maeda K., Nomoto K., 2007, ApJ, 666, 955
O'Halloran B., Satyapal S., Dudik R. P., 2006, ApJ, 641, 795
Panuzzo P. et al., 2007, ApJ, 656, 206
Pilbratt G. L., 2005, in Wilson A., ed., ESA SP-577, Proc. Dusty and Molecular Universe. ESA, Noordwijk, p. 3
Piovan L., Tantalo R., Chiosi C., 2006, MNRAS, 370, 1454
Pipino A., Matteucci F., Borgani S., Biviano A., 2002, NewA, 7, 227
Pipino A., Kawata D., Gibson B. K., Matteucci F., 2005, A&A, 434, 553
Popescu C. C., Tuffs R. J., 2005, AIPC, 761, 155P
Renzini A., 2006, ARA&A, 44, 141
Robson I., Priddey R. S., Isaak K. G., McMahon R. G., 2004, MNRAS, 351, L29
Rowan-Robinson M., Benn C. R., Lawrence A., McMahon R. G., Broadhurst T. J., 1993, MNRAS, 263, 123
Scalo J. M., 1986, Fundam. Cosm. Phys., 11, 1
Shankar F., Salucci P., Granato G. L., de Zotti G., Danese L., 2005, in Merloni A., Nayakshin S., Sunyaev R. A., eds, Growing Black Holes: Accretion in a Cosmological Context. Springer, Berlin, p. 470
Silva L., Granato GL., Bressan A., Danese L., 1998, ApJ, 509, 103 (S98)
Soifer B. T., Neugebauer G., 1991. AJ, 101, 354
Somerville R. S., 2005, in Bender R., Renzini A., eds, Multiwavelength Mapping of Galaxy Formation and Evolution. Springer, Berlin, p. 131
Sugerman B. E. K. et al., 2006, Sci, 313, 196
Swinbank M. et al., 2008, MNRAS, in press (astro-ph/0809.3789)
Temi P., Brighenti F., Mathews W., 2007, ApJ, 666, 222
Thomas D., Maraston C., Bender R., Mendes de Oliveira C., 2005, ApJ, 621, 673
Tuffs R. J., Popescu C. C., Volk H. J., Kylafis N. D., Dopita M. A., 2004, A&A, 419, 821
van den Hoek L. B., Groenwegen M. A. T., 1997, A&AS, 123, 305
Vega O., Silva L., Panuzzo P., Bressan A., Granato G. L., Chavez M., 2005, MNRAS, 364, 1286 Evolution, Lowenthal J. D., Hughes D. H., eds, World Scientific Publishing, Singapore, p. 103
Walter F. et al., 2007, ApJ, 661, 102
Weingartner J. C., Draine B. T., 2001, ApJ, 548, 296
Wiklind T., Dickinson M., Ferguson H. C., Giavalisco M., Mobasher B., Grogin N. A., Panagia N., 2008, ApJ, 676, 781
Wilson T. L., Batrla W., 2005, A&A, 430, 561
Wu Y., Charmandaris V., Hao L., Brandl B. R., Bernard-Salas J., Spoon H. W. W., Houck J. R., 2006, ApJ, 639, 157
Xilouris E. M., Kylafis N. D., Papamastorakis J., Paleologou E. V., Haerendel G., 1997, A&A, 325, 135
Xilouris E. M. et al., 1998, A&A, 344, 868
Xilouris E. M., Kylafis N. D., Paleologou E. V., Papamastorakis J., 1999, A&A, 344, 868
Zhukovska S., Gail H. P., Trieloff M., 2008, A&A, 479, 453
Zubko V., Dwek E., Arendt R. G., 2004, ApJS, 152, 211

This paper has been typeset from a TEX/LATEX file prepared by the author.

Downloaded from https://academic.oup.com/mnras/article/394/4/2001/1203297 by guest on 20 August 2022